Tectonophysics 696–697 (2017) 99–114

Contents lists available at ScienceDirect

Tectonophysics

journal homepage: www.elsevier.com/locate/tecto

The sedimentary and crustal velocity structure of Makarov Basin and adjacent Alpha Ridge

John Evangelatos [a,*], Thomas Funck [b], David C. Mosher [c,1]

[a] Department of Earth Sciences, Dalhousie University, 1355 Oxford Street, Halifax, NS B3H 4J1, Canada
[b] Geological Survey of Denmark and Greenland (GEUS), Øster Voldgade 10, 1350 Copenhagen K, Denmark
[c] Geological Survey of Canada (Atlantic), Natural Resources Canada, Bedford Institute of Oceanography, 1 Challenger Drive, Dartmouth, NS B2Y 4A2, Canada

ARTICLE INFO

Article history:
Received 14 May 2016
Received in revised form 12 December 2016
Accepted 26 December 2016
Available online 28 December 2016

Keywords:
Makarov Basin
Alpha Ridge
Seismic refraction
2D gravity modelling
Large igneous province

ABSTRACT

This study examines the velocity structure of Makarov Basin and the adjacent Alpha Ridge to determine the tectonic origins of these features and link them to the larger Amerasia Basin. Seismic data from sonobuoys distributed along a 650 km-long line extending from Alpha Ridge and across Makarov Basin to the Lomonosov Ridge were analyzed for this purpose. Forward modelling of traveltimes, supported by coincident multi-channel seismic reflection and shipborne gravity data, were used to determine the P-wave velocity structure along the line. The sedimentary cover averages 0.5 km-thick on Alpha Ridge and 1.9 km-thick in Makarov Basin, but reaches up to 5 km-thick at the base of Lomonosov Ridge. Velocities in the sedimentary section range from 1.6 to 4.3 km s^{-1}. As suggested by relatively high velocities, interbedded volcaniclastic or volcanic rock may occur in the deep sedimentary section. The shallow basement of Alpha Ridge (3.3 to 3.6 km s^{-1}) is characterized by semi-continuous high amplitude reflections and is interpreted as volcanic rock possibly intercalated with sedimentary rock. Velocities do not vary significantly in the upper and mid-crustal layers between Alpha Ridge and Makarov Basin. Total crustal thickness decreases from 27 km beneath Alpha Ridge to 5 km-thick in Makarov Basin then thickens to >20 km over a short distance as part of Lomonosov Ridge. The crustal structure of Alpha Ridge is consistent with previous studies suggesting that the Alpha-Mendeleev ridge complex is part of a large igneous province (LIP) with thick igneous crust. The lack of change in crustal velocities between Alpha Ridge and Makarov Basin suggests that the basin, at least partly, either formed during or was influenced by LIP-related magmatism. The rapid transition of crustal thicknesses from Makarov Basin to Lomonosov Ridge supports the interpretation that this section of the ridge is a transform margin.

1. Introduction

While recent geophysical studies (e.g., Mosher et al., 2012; Chian et al., 2016; Shimeld et al., 2016) shed light on the evolution of the southern part of Amerasia Basin, the origins of Alpha Ridge and Makarov Basin, in the northernmost part of Amerasia Basin, remain enigmatic (Fig. 1). This lack of understanding is in part due to the challenges of data acquisition in this remote ice-covered environment and its complex geology. Attempts at deciphering the crustal affinity of the Alpha-Mendeleev ridge complex have led to contradictory models for its origin. Funck et al. (2011) favour an oceanic origin for the Alpha Ridge based on the apparently homogenous crustal velocity structure of the ridge complex, which is similar to other large igneous provinces. Conversely, Døssing et al. (2013) interpreted sub-linear magnetic anomalies in the southern part of the ridge (near Ellesmere Island) as Late Jurassic–Early Cretaceous dykes intruded into thinned continental crust (Fig. 1). The type of crust beneath Makarov Basin is likewise not well known; it may consist of thinned continental crust, as argued for nearby Podvodnikov Basin (Lebedeva-Ivanova et al., 2011), or of thick oceanic crust, as argued by Forsyth and Mair (1984). Jokat and Ickrath (2015) concluded that, along their transect (Fig. 1), almost 50% of Podvodnikov Basin is underlain by extended continental crust of the Lomonosov Ridge. The thinned continental crust terminates against thick igneous crust west of the Mendeleev Ridge.

The objective of this paper is to constrain the origin and relationship between Alpha Ridge and Makarov Basin by studying their sedimentary and crustal structure. To achieve this aim, we rely on new coincident seismic refraction and reflection data supplemented by gravity data. The distribution of data along a line that covers both the Alpha Ridge and Makarov Basin offers the opportunity to address some of the

* Corresponding author at: Department of Earth Sciences, Dalhousie University, 1355 Oxford Street, Halifax, NS B3A 0B1, Canada.
E-mail address: j.evan@dal.ca (J. Evangelatos).
[1] Present address: Center for Coastal and Ocean Mapping, University of New Hampshire, 24 Colovos Road, Durham, NH 03824, USA.

http://dx.doi.org/10.1016/j.tecto.2016.12.026
0040-1951/

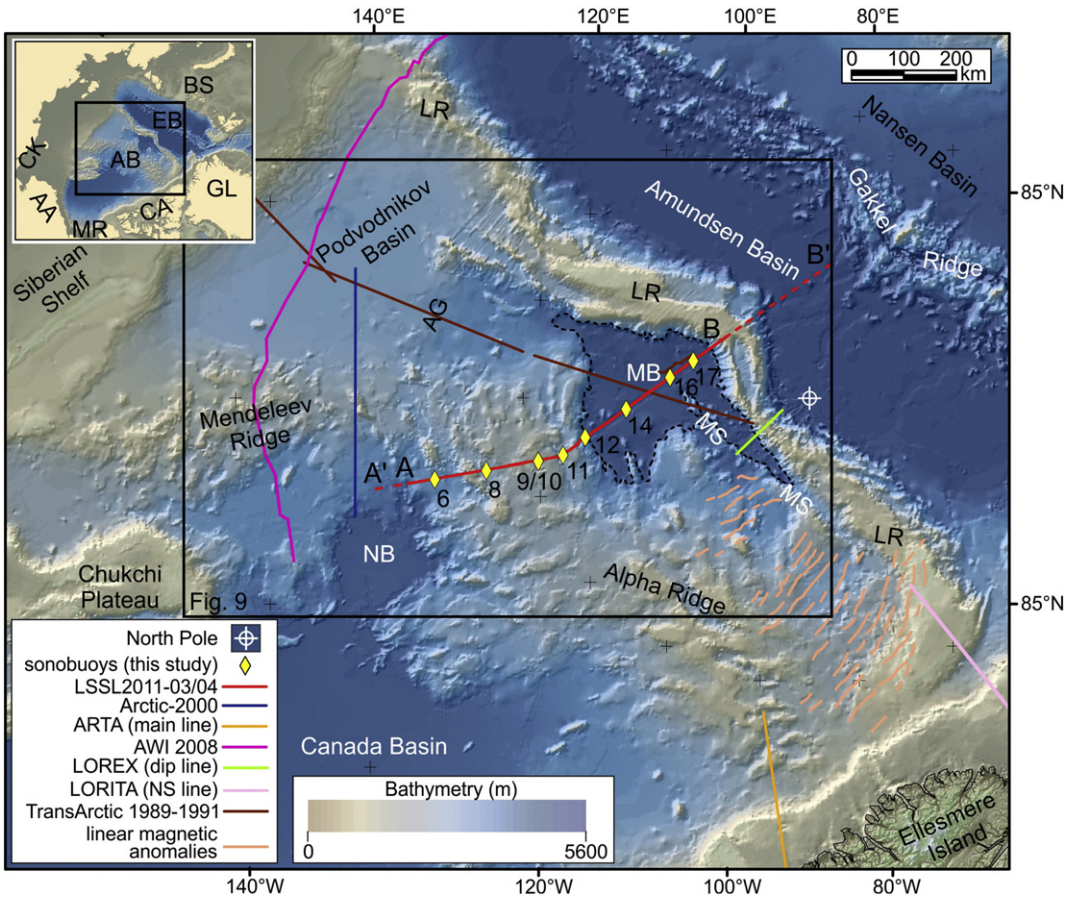

Fig. 1. Colour-shaded bathymetric map of northern Amerasia and Eurasia basins. Labels A and B indicate the end points of the seismic profile shown in Figs. 4 and 5, and labels A′ and B′ are the end points of the gravity model shown in Fig. 7. Makarov Basin is delineated by a dashed black line representing the 3700 m bathymetric contour. Acronyms used in this figure and Figs. 2 and 10 are: AA – Arctic Alaska, AB – Amerasia Basin, AG – Arlis Gap, BS – Barents Shelf, CA – Canadian Arctic margin, CK – Chukotka, EB – Eurasia Basin, GL – Greenland, LR – Lomonosov Ridge, MB – Makarov Basin, MR – Mackenzie River delta, MS – Marvin Spur, NB – Nautilus Basin. (Note that several publications, e.g., Jokat and Ickrath (2015), include Podvodnikov Basin as part of Makarov Basin.) Other studies shown in this figure are: Arctic-2000 (Lebedeva-Ivanova et al., 2006), ARTA (Funck et al., 2011), AWI 2008 (Weigelt et al., 2014; Jokat and Ickrath, 2015), LOREX (Forsyth and Mair, 1984), LORITA (Jackson et al., 2010) and TransArctic 1989–1991 (Lebedeva-Ivanova et al., 2011), and linear magnetic anomalies interpreted by Døssing et al. (2013). Bathymetry and elevation are from the International Bathymetric Chart of the Arctic Ocean (IBCAO), version 3.0 (Jakobsson et al., 2012). The map projection for this figure and other map figures is North Pole Stereographic with a latitude of origin of 75° N and a central meridian of 90° W.

uncertainties regarding the interpretation of these submarine features and thus improve our understanding of the geological history of the Amerasia Basin.

2. Geological setting

Amerasia and Eurasia basins are the two major deep-water basins comprising the Arctic Ocean (Fig. 1). Lomonosov Ridge separates the two basins, extending from the North American shelf off Ellesmere Island and Greenland to the Siberian Shelf. The continental origin of Lomonosov Ridge is confirmed by various investigations (Karasik et al., 1971; Sweeney et al., 1982; Backman et al., 2008; Jackson et al., 2010). Lomonosov Ridge was once part of the palaeo-Barents Shelf, but rifted and drifted away from the shelf in the early Palaeogene due to the opening of Eurasia Basin (Lawver et al., 2002; Pease et al., 2014). The evolution of this basin is documented by well-developed magnetic reversal anomalies (Brozena et al., 2003) associated with Gakkel Ridge, the active spreading centre (Fig. 2). Analysis of the magnetic spreading anomalies indicates that Eurasia Basin expanded at ultra-slow spreading rates throughout its history (Coakley and Cochran, 1998; Jokat and Schmidt-Aursch, 2007).

Amerasia Basin is enclosed by the Canadian Arctic margin, the Alaskan and Siberian shelves, and Lomonosov Ridge (Fig. 1). Bathymetric and sedimentary basins within Amerasia Basin include the Canada, Makarov, Nautilus and Podvodnikov basins. The Alpha-Mendeleev ridge complex and the Chukchi Plateau are also part of Amerasia Basin. The Alpha-Mendeleev ridge complex extends from the Canadian Arctic margin near Ellesmere Island to the Siberian Shelf, separating Makarov and Podvodnikov basins from the rest of Amerasia Basin. Makarov Basin is bounded almost entirely by Alpha and Lomonosov ridges, and is connected to Podvodnikov Basin through the Arlis Gap (Fig. 1). The processes that shaped Amerasia Basin and formed the various physiographic features within the basin are seemingly complex. Consequently, new geoscientific data are needed to unravel the details of the geological evolution of Amerasia Basin. For example, unlike Eurasia Basin, the existence of seafloor spreading in Amerasia Basin, as evidenced by magnetic isochrons, is contested (Vogt et al., 1982; Grantz et al., 2011; Chian et al., 2016). Such uncertainty has led to numerous plate-reconstruction models for the origin of Amerasia Basin (summarized in Lawver and Scotese [1990] and Cochran et al. [2006]). The widely supported "rotational" model, championed by Grantz et al. (1979, 1998, 2011), amongst others, attributes opening of Amerasia Basin to counter-clockwise rotation of the Arctic Alaska–Chukotka microplate away from the Canadian Arctic margin about a pole of rotation in the area of the Mackenzie River delta (Fig. 2). A linear gravity low that bisects Canada Basin (Laxon and McAdoo, 1994), and is shown in seismic reflection profiles to coincide with a negative basement structure (Mosher et al., 2012), is interpreted as an extinct spreading centre

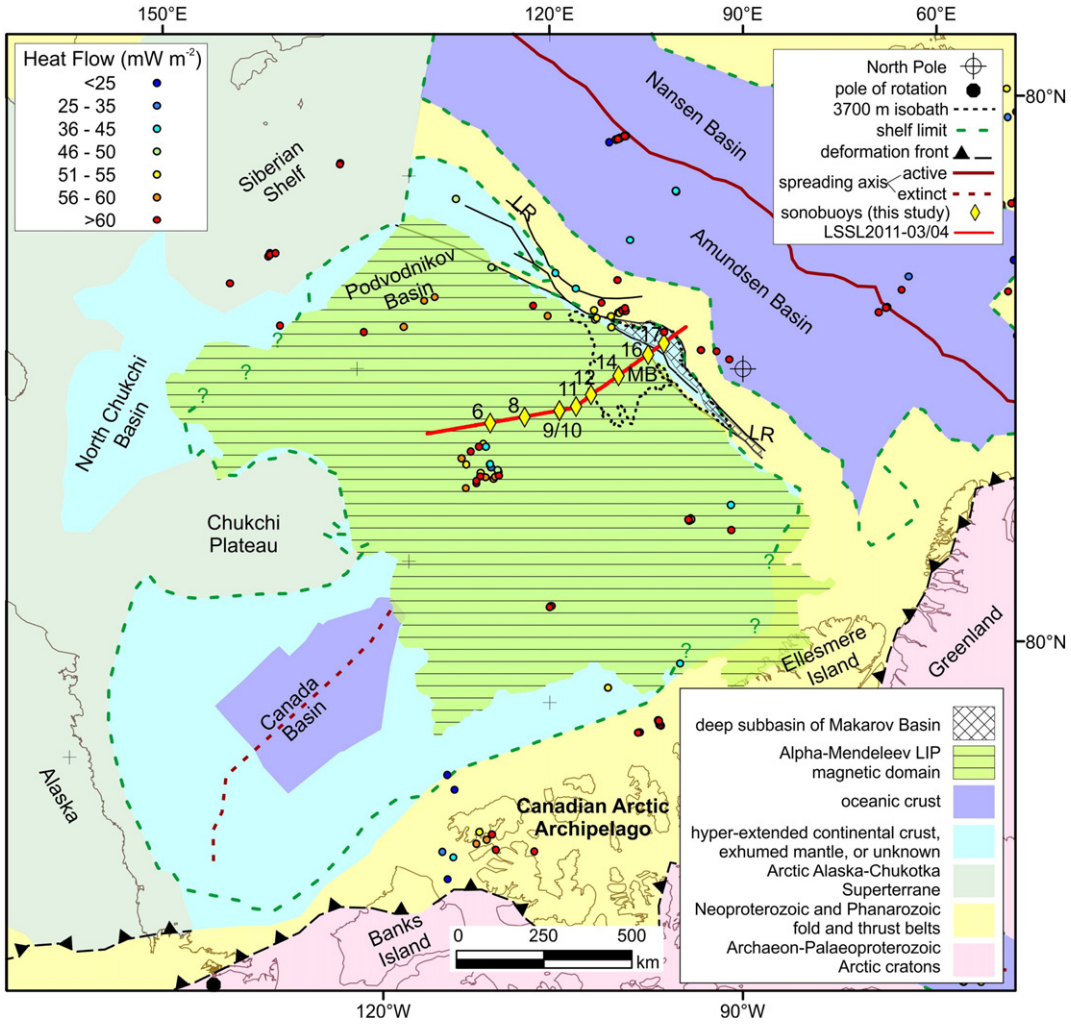

Fig. 2. Simplified tectonic map of Amerasia Basin and surrounding regions is shown (after Pease et al. [2014]). Other sources shown in the figure are: marine heat flow data (data available at http://www.heatflow.und.edu; see also Pollack et al. [1993]), pole of rotation for opening of Amerasia Basin (Grantz et al., 1979), sonobuoys and seismic line LSSL2011-03/04 (this study), 3700 m isobath produced using the IBCAO compilation (Jakobsson et al., 2012), deep subbasin of Makarov Basin (Evangelatos and Mosher, 2016), Alpha-Mendeleev LIP magnetic domain (Saltus et al., 2011) and oceanic crust in Canada Basin (Chian et al., 2016).

(Fig. 2). This interpretation supports the rotational model. The northern extent of this gravity anomaly terminates at the edge of the magnetic domain associated with the Alpha-Mendeleev Large Igneous Province (LIP) (Saltus et al., 2011; Fig. 2). Whether the spreading centre actually terminates at that location or is masked by the LIP is undetermined. The tectonic model of Grantz et al. (2011), supported by morphological evidence presented by Cochran et al. (2006) and Evangelatos and Mosher (2016), suggests it propagated to Lomonosov Ridge.

Alpha Ridge and Mendeleev Ridge form a distinct physiographic entity that spans 1800 km from the Siberian Shelf to the Canadian Arctic shelf off Ellesmere Island. The Alpha-Mendeleev ridge complex is characterized by elevations up to 2000 m above the adjacent Canada and Makarov basins, and its width varies from 200 to 600 km along its length (Fig. 1). The ridge complex and surrounding areas exhibit a chaotic pattern of alternating high and low amplitude and short wavelength magnetic anomalies (Gaina et al., 2011). Saltus et al. (2011) defined this region as the Alpha-Mendeleev LIP magnetic domain. These authors suggested a large magnetic thickness based on a pseudogravity transformation. The interpretation of the Alpha-Mendeleev ridge complex as a LIP is supported by basalt recovered in dredges, cores and drilling (Van Wagoner et al., 1986; Andronikov et al., 2008; Jokat et al., 2013; Petrov et al., 2016), its magnetic signature (Vogt et al., 2006) and the seismic velocity structure of its crust (e.g., Funck et al., 2011). Mineral textures from volcaniclastic samples dredged from the Alpha Ridge during the CESAR (Jackson et al., 1985) and HEALY0805 (Mayer and Armstrong, 2008) expeditions indicate shallow-water eruptions (< 800 m; Van Wagoner et al., 1986). The origin of these ridges, however, is still not clear (Dove et al., 2010). The recognition of mafic volcanism of Cretaceous age in the circum-Arctic led researchers to include the ridge complex as part of the greater High Arctic Large Igneous Province (HALIP) (Maher, 2001). While early HALIP-related magmatic suites are predominantly tholeiitic, later magmatism is more alkaline (Tegner et al., 2011). The genetic relationship between these different suites and their connection to Arctic tectonics is not known (Estrada, 2015). Various authors have proposed that a mantle plume, focused offshore of Ellesmere Island, initiated rifting in Amerasia Basin and sustained over ~50 Myr of circum-Arctic magmatism (Embry and Osadetz, 1988; Buchan and Ernst, 2006; Døssing et al., 2013).

The rhomboid-shaped Makarov basin is approximately 300 by 400 km wide. The abyssal plain of Makarov Basin is well-outlined by the 3700 m bathymetric contour (Fig. 1) with seafloor depths reaching down to 4000 m. Marvin Spur is a linear ridge in northern Makarov Basin that trends sub-parallel to Lomonosov Ridge (Fig. 1). Isolated basement protrusions also occur near Alpha Ridge in the southern part of the basin. Seismic refraction studies (Forsyth and Mair, 1984; Lebedeva-Ivanova et al., 2011) and interpreted magnetic reversal anomalies near the Canadian Arctic margin (Døssing et al., 2013) are compatible with normal oceanic crust in Makarov Basin (Figs. 1 and

2). Cochran et al. (2006), Doré et al. (2015) and Evangelatos and Mosher (2016) showed evidence that Makarov Basin, at least in part, formed as a result of transtensional tectonics adjacent to the palaeo-Barents Shelf (now Lomonosov Ridge) during opening of Amerasia Basin. Based on studies conducted onshore, Miller and Verzhbitsky (2009) argued that the Alpha-Mendeleev ridge complex rifted off the margin of the palaeo-Barents Shelf, thus forming the Makarov and Podvodnikov basins in between these ridges. The results of this study can elucidate the geological connection between these submarine features.

3. Methodology

3.1. Data acquisition

Coincident seismic refraction and multi-channel seismic (MCS) data were acquired in Amerasia Basin in 2011 (Mosher, 2012). During seismic operations, data were collected aboard the Canadian Coast Guard Ship *Louis S. St-Laurent*. Meanwhile, the US Coast Guard Cutter *Healy* broke ice ahead of the *Louis S. St-Laurent*. This configuration allowed for continuous seismic acquisition in heavy ice cover (Mayer and Armstrong, 2011; Mosher, 2012; Mosher et al., 2013). Expendable sonobuoys,[2] model 53C from Ultra-Electronics, were deployed either off the stern of the *Louis S. St-Laurent* or ahead of the ship via helicopter. Upon deployment, a sonobuoy released a hydrophone that suspended 60 m below the water surface. The signals recorded by the hydrophone were transmitted to the vessel by radio and digitally recorded in SEG-Y format. The sonobuoys were not fitted with a navigational device, and, once deployed, drifted freely with the ice pack. The maximum operating time for a sonobuoy is about eight hours, during which the ship generally sailed between 35 and 50 km. Straight lines and a constant ship speed were not possible in heavy ice. Seismic energy was not observed beyond offsets of 27 to 43 km (Fig. 3) with the exception of sonobuoy 9 that only had a maximum offset of 19 km. Source energy is inferred to control maximum offsets in Alpha Ridge due to the observation of the direct wave beyond the last recognizable arrival associated with a crustal phase. For Makarov Basin, the maximum offsets for the direct wave and crustal phases are close (<5 km apart), suggesting that radio range is the limiting factor in this case. Fourteen sonobuoys were deployed along a line LSSL2011-03/04 extending from Alpha Ridge and across Makarov Basin to the Amerasian flank of the Lomonosov Ridge (Fig. 1). Of those deployments, nine sonobuoy records are included in this study. The five excluded sonobuoys either malfunctioned or returned data only for very short offsets before failing. Water depths along the line range from about 1500 m on Alpha Ridge to almost 4000 m in Makarov Basin.

The MCS data were acquired using a 16-channel digital streamer with a group spacing of 6.25 m. The streamer was 230 m long. The seismic source was arranged as a three-airgun array with a total volume of 1150 in^3 (~19 l). Towed at 11.5 m below sea surface, this configuration yielded a frequency spectrum of 5 to 60 Hz, resulting in a maximum vertical resolution of about 8 m (1/4 wavelength). Firing on distance was not practical in ice. The firing interval was adjusted according to water depth to avoid interference from multiple reflections. This adjustment resulted in a variable firing interval, ranging between 14 and 19 s. Because of the irregular geometry and shot interval, traces were gathered into bins of 25 × 25 m intervals along a curved line for MCS stacking. Processing of the MCS data is described in Shimeld (2011) and Mosher et al. (2013).

In addition to the seismic acquisition system, both the *Louis S. St-Laurent* and the *Healy* were equipped with Bell BGM-3 gravimeters. Gravity data recorded on board the *Louis S. St-Laurent* are less affected by noise. This result is because the *Healy* typically broke ice ahead of the *Louis S. St-Laurent*, thus sustaining significantly more accelerations that led to more noise on the gravimeter on board the Healy. Our study primarily uses gravity data from the *Louis S. St-Laurent* (Mosher, 2012). Further details on geophysical acquisition are provided in Mosher (2012) and Mosher et al. (2013). The seismic reflection data are publicly available through the Geological Survey of Canada (Mosher et al., 2016).

3.2. Seismic refraction and gravity data processing

Static corrections were applied to the seismic data to account for the trigger/gun firing delay. Data were de-spiked using a spike-zeroing filter (Stanghellini and Bonazzi, 2002). As the sonobuoys were not equipped with a navigational device, the source–receiver offsets were derived using the traveltime of the direct wave. For this correction, we applied the following quadratic equation:

$$X = a + bT + cT^2,$$

where X is the offset in km, T represents the traveltime of the direct wave in seconds, and coefficients a, b and c are −0.006, 1.441 and 0.00075, respectively (Lebedeva-Ivanova and Lizarralde, 2011). This formula was empirically derived using CTD (conductivity, temperature, depth) measurements in High Arctic waters. Most records from sonobuoys have a high signal-to-noise ratio.

Barring periods of instrument failure, marine gravity data were acquired continuously during the expedition. The raw data were corrected for Eötvös effects and latitude. The data were then filtered with a 2-min Gaussian moving-window to correct for ship heave and re-sampled at 1 min intervals. Long-term instrument drift was addressed by tying back to an absolute gravity station at the end of the cruise (Mosher, 2012). Finally, the gravity data were de-spiked with an 8-min median filter and reduced to free-air gravity anomalies.

3.3. Geophysical modelling

3.3.1. Modelling seismic velocities

The development of a two-dimensional representation of the subsurface velocity structure requires that the calculated arrival times of reflected and refracted seismic waves, based on the velocity model, match the observed arrival times on wide-angle reflection and refraction data within the range of the data uncertainty. Observed arrival times for the various phases were determined using ZPLOT, a program designed for interactive picking of traveltimes (Zelt, 1994). Calculated arrival times were derived by forward modelling using RAYINVR, a seismic program developed by Zelt and Smith (1992) that uses the ray-tracing technique. The velocity model divides the subsurface into distinct layers (Figs. 4 and 5) defined by boundary and velocity nodes. Velocity gradients between nodes are linear.

The sonobuoy position is assumed to be constant; however, variable relief at the seafloor and in subsurface structure can introduce errors as the sonobuoy drifted. If the drift of the buoy is along the shot line, the effects can be corrected by using a variable sonobuoy position in the modelling. However, the drift presumably has an unknown component perpendicular to the line where information on water depth or deeper structures is unavailable. For this reason, only the offset correction between the sonobuoys (source) and the shots (receiver) was applied.

Seismic velocities for a given phase were determined one station at a time and each layer in the velocity model was analyzed in sequence from shallowest to deepest. The final model is the result of multiple iterations (Figs. 3, 4 and 5). Converted shear waves were not included in this study. The depth of the seafloor was measured with a Knudsen 12 kHz echo sounder mounted on the hull of the *Louis S. St-Laurent* (Mosher, 2012). The layer boundaries identified at individual sonobuoys were converted from depth to two-way traveltime (TWTT) to check for correlation with the seismic reflections on the MCS record.

[2] For brevity, we refer to sonobuoys according to their order of deployment rather than their full name (e.g., SB2011-6 is simply sonobuoy 6; refer to Chian and Lebedeva-Ivanova [2015]).

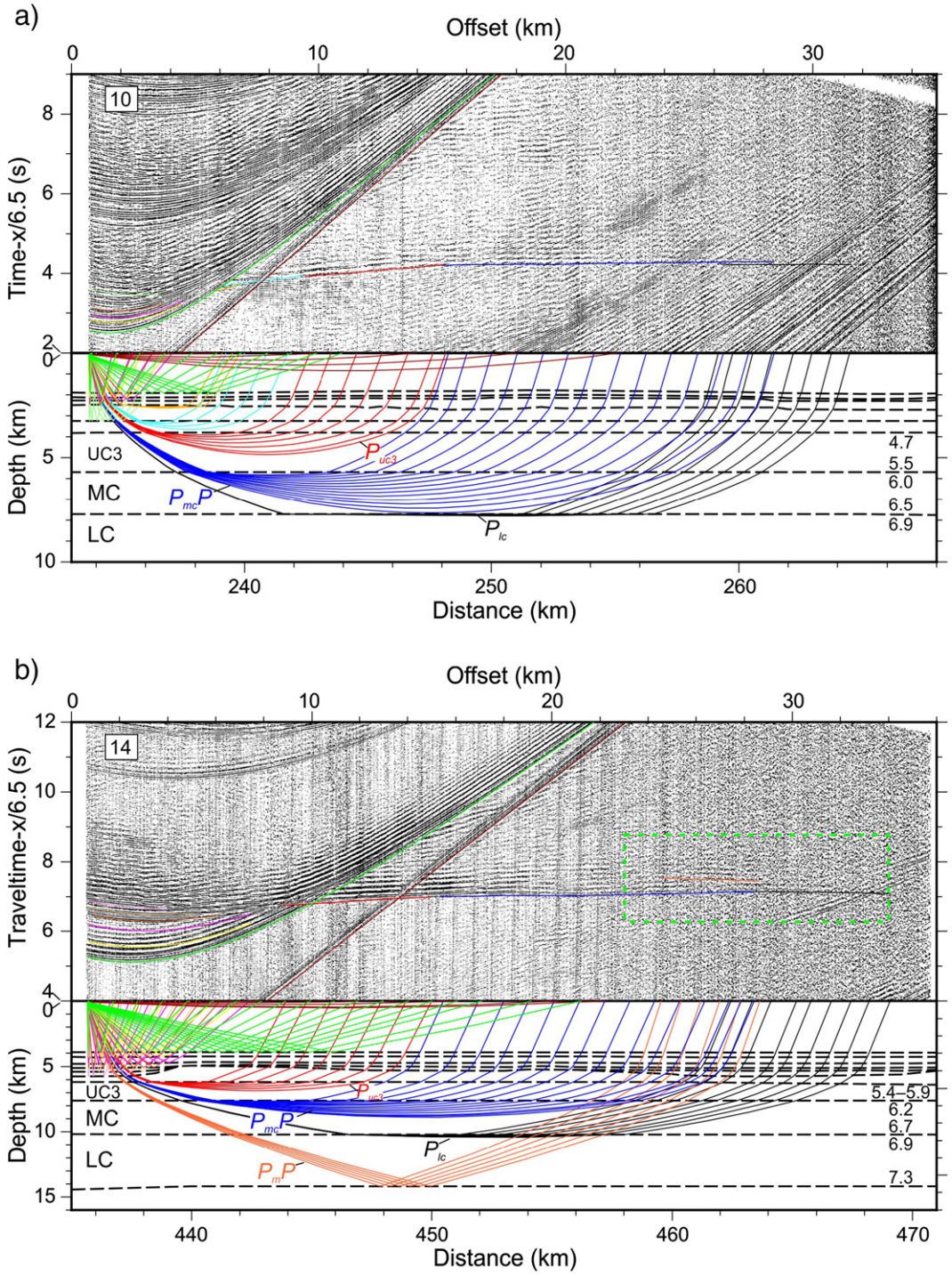

Fig. 3. Records and modelling of sonobuoy stations a) 10 (Alpha Ridge), and b) 14 (Makarov Basin) are depicted. The top panels show the seismograms with overlain calculated traveltimes, and the bottom panels outline the raypaths through the velocity model. The green dashed box outlines the portion of station 14 shown in Fig. 6. Names and P-wave velocities (km s^{-1}) for select crustal phases and layers are labelled (refer to Section 4). Displayed seismic records were band-pass filtered between 4 and 20 Hz. Deployment positions are shown in Fig. 1.

Where there is such a correlation, the MCS record was used to define the detailed geometry of these layer boundaries, which would not have been possible with the resolution of the data from sonobuoys alone. Although some coherent signal is present within basement, seismic reflection imaging was inadequate to resolve upper crustal interfaces. Below the imaging depth of the MCS data, therefore, boundaries were constrained by refraction and wide-angle reflection data and represented as horizontal surfaces. It is difficult to independently assess the geometry of intra-crustal layer boundaries without reversed ray coverage. Near Alpha and Lomonosov ridges, however, relief was added to deeper layer boundaries to fit the free-air gravity anomalies. The crustal velocity structures derived by Funck et al. (2011) (Alpha Ridge), Lebedeva-Ivanova et al. (2011) (Makarov Basin) and Poselov et al. (2012) (Lomonosov Ridge) were used as guides only for early iterations of the velocity structure at deep crustal levels. As there is no overlap in ray coverage between neighbouring stations (Fig. 4), the transition in velocity across layer segments is smoothed (Fig. 5).

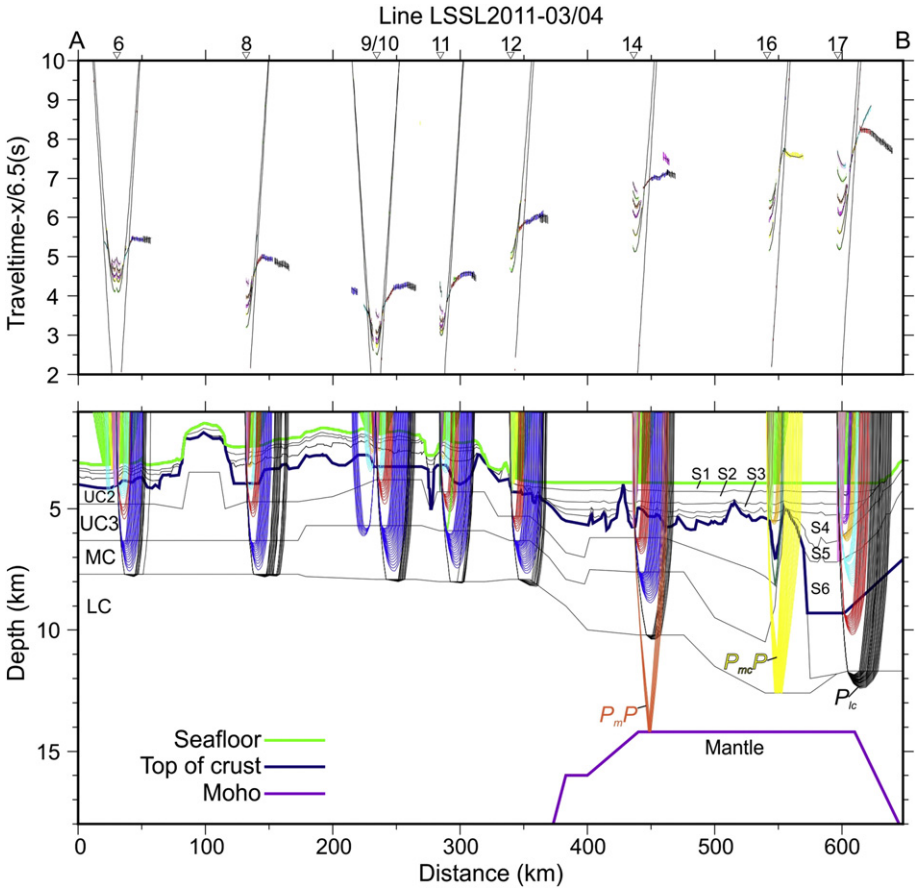

Fig. 4. (Top panel) observed traveltime picks are shown with the calculated traveltimes overlain. Traveltime picks are represented by vertical error bars. (Bottom panel) raypath diagrams from velocity modelling. Labels for select phases and layers are shown (refer to Section 4).

3.3.2. Error analysis of velocity model

To quantify the accuracy of the velocity model, a formal error analysis was carried out in which the root-mean-square of the misfit between observed and modelled traveltimes (rms error) was calculated (Table 1). Uncertainties were assigned to traveltime picks based on visual inspection, which relied on the frequency content of the phase

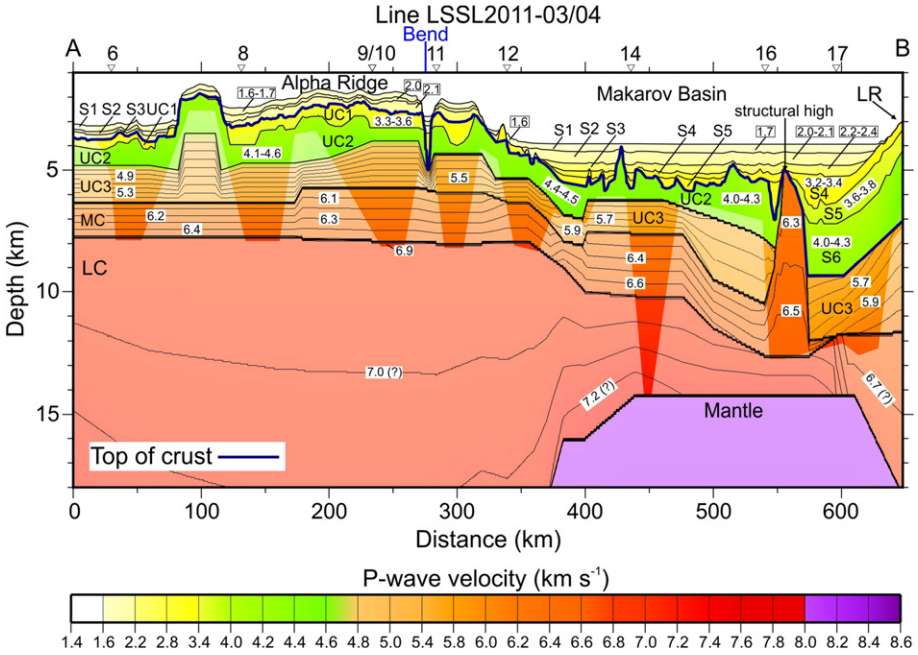

Fig. 5. P-wave velocity model for line LSSL2011-03/04 is shown. Pale colours indicate sections unconstrained by MCS or data from sonobuoys. Ray coverage is shown in Fig. 4. "Bend" marks the location along line LSSL2011-03/04 where the orientation of the line changes (Fig. 1). Velocities are specified in km s^{-1}.

Table 1
Results of error analysis for the individual phases are listed. n, t_{rms}, and χ^2 are the number of observed traveltime picks, the root-mean-square difference between observed and calculated traveltimes, and normalized χ^2. Column "Identification" describes which stations were defined for a particular phase. P_{water} and $P_{water}P$ are the direct wave (water wave) and seafloor reflection, respectively. All other phases are defined in Section 4.

Phase	Identification	n	t_{rms} (s)	χ^2
P_{water}	All	1583	0.022	0.730
$P_{water}P$	All	1685	0.018	0.513
P_{S1}	None	–	–	–
$P_{S1}P$	All	460	0.026	0.460
P_{S2}	17	6	0.026	0.496
$P_{S2}P$	All, except 12	356	0.025	0.284
P_{S3}	8	6	0.037	0.255
$P_{S3}P$	All, except 12	315	0.028	0.337
P_{S4}	17	27	0.030	0.584
$P_{S4}P$	12, 14, 16, 17	183	0.027	0.244
P_{S5}	16, 17	56	0.017	0.152
$P_{S5}P$	14, 17	77	0.027	0.171
P_{S6}	17	74	0.022	0.186
$P_{S6}P$	None	–	–	–
P_{uc1}	6, 8, 9, 10, 11	52	0.032	0.323
$P_{uc1}P$	6, 8, 9, 10, 11	138	0.028	0.260
P_{uc2}	6, 8, 9, 10, 11	177	0.022	0.297
$P_{uc2}P$	11	16	0.026	0.110
P_{uc3}	All, except 9, 16	327	0.025	0.189
$P_{uc3}P$	11	16	0.033	0.318
P_{mc}	All, except 16, 17	649	0.025	0.179
$P_{mc}P$	16	120	0.036	0.372
P_{lc}	All, except 9, 16	471	0.038	0.234
P_mP	14	37	0.026	0.097
P_m	None	–	–	–
All phases	All	6848	0.025	0.436

being picked and interfering signal from other phases. Uncertainties ranged from 20 ms to 80 ms with an average value of 41 ms. As the signal-to-noise ratio increases with offset, the pick uncertainty increased accordingly. χ^2 quantitatively represents the fit between model and data. The ideal χ^2 is unity (Zelt and Smith, 1992). Values <1 indicate over-fit of the data, but can also be caused by an overestimation of pick uncertainty. Perfectly fit data have $\chi^2 = 0$. In practice, low values for χ^2 were fairly simple to obtain as the experiment has no reversed ray coverage.

Because uncertainty is not represented entirely by χ^2, uncertainty in velocity and depths to layer boundaries are also estimated by sensitivity analysis. This process involved noting the rms error of a given phase after systematically varying depth and velocity. This information is used to identify the best values (i.e., pairs with minimum RMS error) for boundary depths and layer velocities and to estimate uncertainty. Table 2 lists the uncertainties assigned to the sedimentary and upper crustal layers.

Table 2
General properties of sedimentary layers S1 to S6 and upper crustal layers UC1 to UC3 are listed. Alpha Ridge is from 0 to 340 km along line and Makarov Basin is from 340 to 625 km along line (Fig. 5).

Layer	Velocity (km s^{-1})	Average thicknesses for Alpha Ridge (km)	Average thicknesses for Makarov Basin (km)	v_{error} (km s^{-1})	d_{error} (km)
S1	1.6–1.8	0.2	0.3	0.1	0.05
S2	2.0–2.2	0.1	0.4	0.1	0.05
S3	2.1–2.5	0.2	0.3	0.1	0.05
S4	2.8–3.4	–	0.3	0.2	0.1
S5	3.1–3.8	–	0.3	0.2	0.1
S6	3.9–4.3	–	0.4	0.2	0.2
UC1	3.3–3.6	0.4	–	0.2	0.1
UC2	4.0–4.6	1.1	1.3	0.2	0.2
UC3	4.8–6.0	1.6	1.5	0.2	0.3

v_{error}: uncertainty of velocity.
d_{error}: uncertainty of top layer boundary.

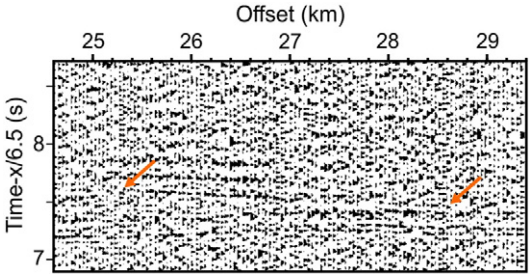

Fig. 6. Record from station 14 centred on the P_mP reflection phase. Orange arrows point to the ends of the phase.

3.3.3. Two-dimensional gravity modelling

The base of the crust is poorly resolved by the data from sonobuoys (Fig. 4). Depth to the Mohorovičić discontinuity (Moho) along line LSSL2011-03/04 is seismically constrained based on P_mP reflections from station 14 (Fig. 6). In addition, at the intersection with line TransArctic 1989–1991 (Figs. 1 and 7), Moho is constrained at a depth of 14.0 ± 1.5 km, as determined by P_mP and P_n phases (Lebedeva-Ivanova et al., 2011). Elsewhere along the line, the Moho depth was adjusted by gravity modelling to fit the long wavelength component of the observed gravity.

Our velocity model was converted to a density model using the empirical relationship derived by Osler (1993) from the work of Ludwig et al. (1970):

$$\rho = -2.83Vp^4 + 70.4Vp^3 - 598Vp^2 + 2230Vp - 700,$$

where Vp and ρ are P-wave velocity (in km s^{-1}) and density (in kg m^{-3}), respectively. Mantle density is assumed to be 3300 kg m^{-3}. The gravitational response of the density model is calculated according to the method of Talwani et al. (1959) and then compared with the shipborne gravity (Fig. 7). The density model was extended on either end of the velocity model to account for edge effects (Fig. 1). Seafloor depths were extracted from the International Bathymetric Chart of the Arctic Ocean (IBCAO version 3.0 by Jakobsson et al. [2012]). The observed gravity for the section of the model extending into Nautilus Basin was fit by incorporating seafloor depths, setting sedimentary layer boundaries parallel the seafloor down to the basement and extending deeper layer boundaries horizontally southward. For the section extending across Lomonosov Ridge and into Amundsen Basin, the model incorporates seafloor depths and seismic data constrain the sedimentary succession and crust (Jokat et al., 1992; Jokat et al., 1995; Weigelt and Jokat, 2001; Jackson et al., 2010; Poselov et al., 2012; Døssing et al., 2014).

4. Results and interpretations

A velocity model representing the earth structure extending from Alpha Ridge through Makarov Basin was developed. It is divided into the sedimentary cover, crust and mantle (Fig. 5). The distinction between sedimentary cover and crust is largely based on the MCS data. Table 2 lists the velocity range, average thickness and estimated uncertainties of modelled velocity and the top of layer boundaries for sedimentary and upper crustal layers.

4.1. Sedimentary layers

MCS reflection data in this study typically recover coherent signals down to 1.5 s TWTT (~1.5 km) below seafloor along Alpha Ridge, and down to 3.5 s TWTT (~5 km) below seafloor in Makarov Basin (Fig. 8). These data clearly resolve the base of the sedimentary cover and the upper parts of the crust. We identify three and six sedimentary layers

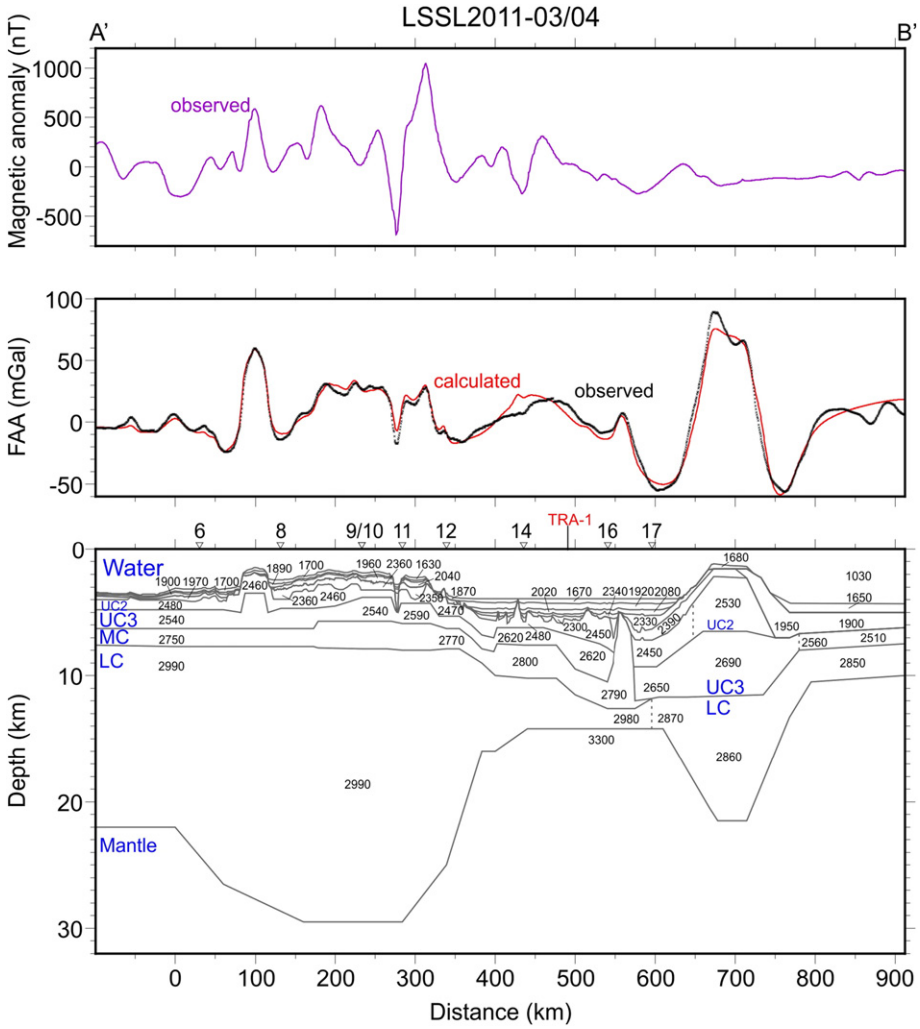

Fig. 7. Two-dimensional gravity model for line LSSL2011-03/04 is shown. (Top panel) observed magnetic anomaly data extracted from a grid. (Middle panel) observed free-air gravity anomaly (FAA) is compared to calculated gravity. (Bottom panel) subsurface gravity model shown with representative densities specified in kg m^{-3}. "TRA-1" marks the cross-point with line TransArctic 1989–1991 (Fig. 10). FAA data are a combination of shipborne gravity (Mosher, 2012) and the compilation of Gaina et al. (2011). Magnetic data are a combination of compilations by Brozena et al. (2003) and Gaina et al. (2011). Refer to Fig. 1 for location.

for Alpha Ridge and Makarov Basin, respectively (Fig. 5). Refractive phases for shallow sedimentary layers (P_{s1} to P_{s3}) are typically secondary arrivals. They are difficult to identify because of interference with reverberations of first arrivals. In Makarov Basin, refractive phases for the deep sedimentary layers (P_{s4} to P_{s6}) are first arrivals and, therefore, easier to identify. Layer boundaries constrained by reflective phases ($P_{s1}P$ to $P_{s6}P$) correlate with continuous high amplitude reflections in MCS data.

Velocities in the sedimentary layers range from 1.6 km s^{-1} to 4.3 km s^{-1} (Table 2). These velocities are used to convert seismic reflection data from traveltime to depth. Average thickness of the sedimentary cover is 0.5 km for Alpha Ridge and 1.9 km for Makarov Basin with a maximum of up to 5 km near Lomonosov Ridge.

Sedimentary layers S1, S2 and S3 exhibit velocities of 1.6–2.2 km s^{-1} on Alpha Ridge, and 1.6–2.5 km s^{-1} in Makarov Basin. The combined sedimentary thickness for these three layers ranges from 0 to 1.3 km, with the thickest sections found in Makarov Basin. Layers S1 to S3 coincide with seismic reflection facies (Fig. 8) that were interpreted as hemipelagic to pelagic deposits (Bruvoll et al., 2010; Evangelatos and Mosher, 2016) and/or distal turbidites (Johnson et al., 1990; Langinen et al., 2009). The drape-like character of these layers supports either of these interpretations.

Sedimentary layer S4 is present only in Makarov Basin (Fig. 5). Velocities vary between 2.8 and 3.4 km s^{-1} with an average layer thickness of 0.3 km and a maximum of 1.4 km. The upper part of S4 (above horizon L; Fig. 8b) corresponds to units 3 and 4a from Evangelatos and Mosher (2016), who interpreted these units to consist of hemipelagic sediments. The lower part of S4 (below horizon L; Fig. 8b) coincides with Unit 2 (Evangelatos and Mosher, 2016) and exhibits basinward dipping reflections that grade into more horizontally stratified reflections at the base of the Lomonosov Ridge. This part of S4 consists mainly of sediments that were deposited in Makarov Basin and on the slope of Lomonosov Ridge while the latter was still connected to the Barents Shelf (Evangelatos and Mosher, 2016).

Velocities of 3.1 to 4.3 km s^{-1} were determined for layers S5 and S6 (Fig. 5). These layers are observed mainly in the deep subbasin of Makarov Basin (Fig. 8b). They range in thickness from 0 to 3.4 km with an average of 0.7 km. Layer S5 has high amplitude, semi-continuous and stratified reflections (Fig. 8b). Layer S6 is similar, but of lower amplitude and less coherency. The two layers correspond to Unit 1 of Evangelatos and Mosher (2016), and are interpreted as a mix of volcanic and sedimentary material based on their acoustic character.

The base of the sedimentary cover is mapped along a high amplitude reflection that is traceable across line LSSL2011–03/04 (Fig. 8). This horizon separates relatively continuous and stratified seismic facies, interpreted as sedimentary layers S1 to S6, from underlying semi-continuous seismic facies that have high amplitudes and poor to moderate coherence (Fig. 8). Shallow intra-basement reflections appear offset by faulting.

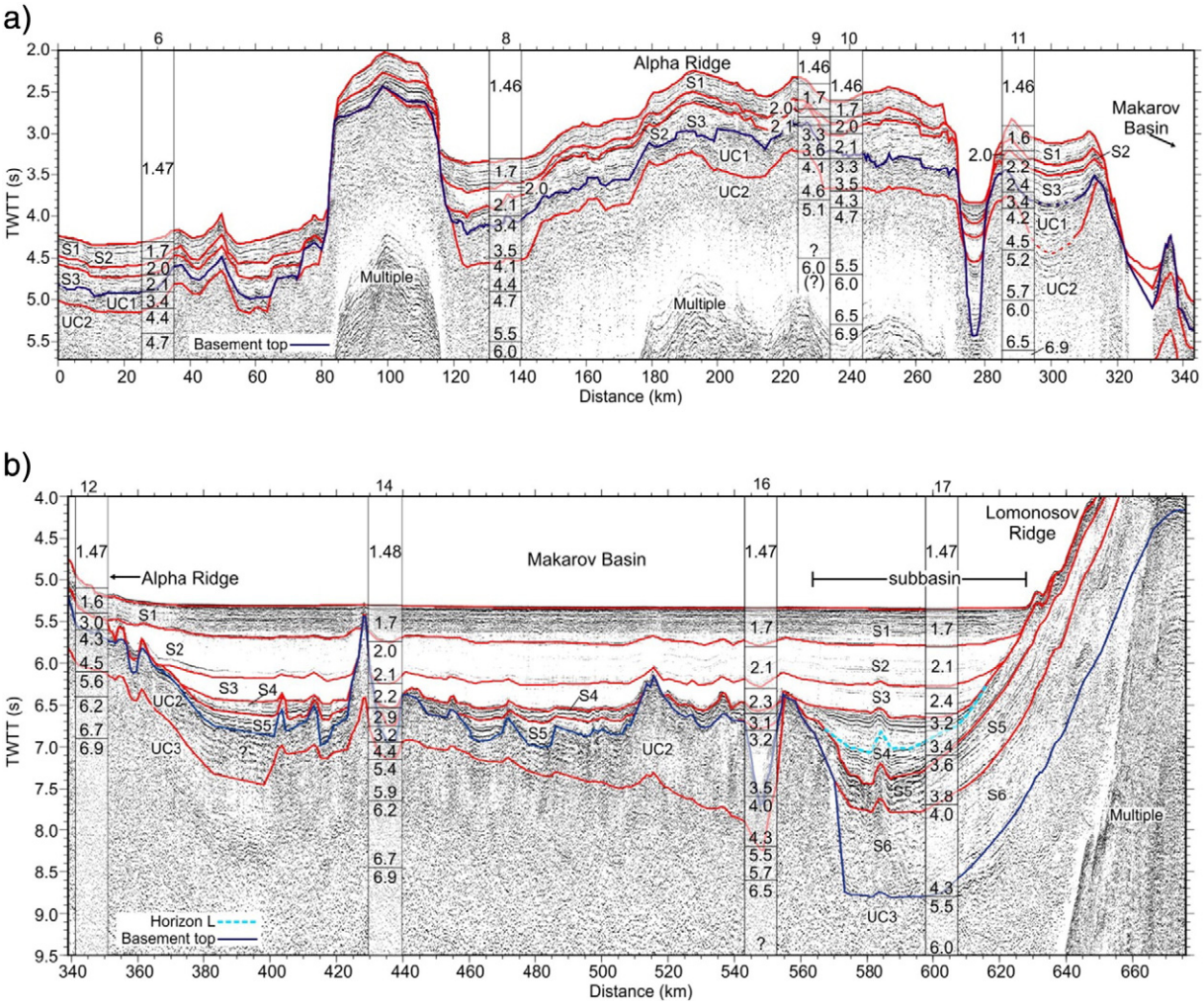

Fig. 8. Multi-channel seismic profiles along line LSSL2011-03/04 are shown from a) Alpha Ridge and b) Makarov Basin. Layer boundaries from the velocity model, displayed as red lines, were converted from depth to time. Horizon L demarcates the boundary between units 2 and 3 from Evangelatos and Mosher (2016). Basement top is defined based on changes in acoustic character. Annotations for P-wave velocities are specified in km s^{-1}.

4.2. Upper crustal layers

The velocity model of this study distinguishes five crustal layers. Three layers, UC1, UC2, and UC3, have velocities less than or equal to 6 km s^{-1} and together define the upper crust. The upper crust is resolved by refractive (P_{uc1}, P_{uc2}, and P_{uc3}) and reflective ($P_{uc1}P$, $P_{uc2}P$ and $P_{uc3}P$) phases.

Layer UC1 has an average thickness of 0.4 km and is only observed on Alpha Ridge. UC2 is present from 0 to 560 km along the line and has a variable thickness of 0.5 to 2.7 km, excluding a filled valley between 272 and 282 km distance along line (Fig. 8a). UC3 is the lower part of the upper crust. Its thickness is between 0.8 and 2.8 km. On Alpha Ridge, velocities for UC1, UC2 and UC3 are 3.3–3.6 km s^{-1}, 4.1–4.6 km s^{-1} and 4.8–5.6 km s^{-1}, respectively. In Makarov Basin, between 360 km and 560 km along line (Fig. 5), velocities for layers UC2 and UC3 are 4.4–4.5 km s^{-1} and 5.4–6.0 km s^{-1}, respectively. These velocities are derived solely from station 14, as ray coverage in the upper crust of station 16 is poor. Beneath the deep subbasin (560 to 625 km along line; Fig. 5) and near the slope of Lomonosov Ridge, layer UC3 has a velocity of 5.5–6.0 km s^{-1}.

Although P-wave velocities for layer UC1 overlap with different types of sedimentary rock (Sheriff and Geldart, 1995), we suggest that UC1 is composed of volcaniclastic or volcanic rock possibly intercalated with sedimentary rock. This interpretation is based on its stratified and semi-continuous seismic character (Fig. 8a). Such seismic facies are interpreted as sills, tuff and/or volcanic flows in other parts of Alpha Ridge and Mendeleev Ridge (Bruvoll et al., 2012). Recovery of volcanic/volcaniclastic rocks from shallow coring (Jokat et al., 2013) and dredging (Mayer and Armstrong, 2012; Mayer et al., 2016) from disparate locations corroborate this interpretation. Correlation between basement topography and high amplitude magnetic anomalies at Alpha Ridge (Vogt et al., 1979; Kovacs and Vogt, 1982) implies that the upper crust is composed of mafic rock, which is typically more magnetic than felsic rock (Hunt et al., 1995). High porosity in the basalts (Wilkens et al., 1991) may also contribute to the lower than expected velocities.

The acoustic signature of UC2 is amorphous, possibly due to lithological change or lack of acoustic energy at this imaging depth. We interpret the upper crust of Alpha Ridge and part of Makarov Basin (360 to 560 km along line; Fig. 5) as a thick magmatic succession (with possible intercalated sedimentary rock in the shallow parts).

4.3. Mid- and lower crustal layers

The middle (MC) and lower (LC) crustal layers are constrained by refractions P_{mc} and P_{lc}, respectively. On Alpha Ridge, the mid-crustal layer

(6.0–6.5 km s^{-1}) has a thickness of 1.4–2.1 km. In Makarov Basin, from 360 to 540 km, these values are 6.2–6.7 km s^{-1} and 1.1–2.6 km, respectively. Uncertainties in mid-crustal velocities are estimated to be ± 0.3 km s^{-1}. The base of layer MC has an uncertainty of ± 0.4 km. Layer MC pinches out beneath the slope of Lomonosov Ridge (575 to 605 km along line; Fig. 5).

The rays associated with the observed P_{lc} arrivals sample only the uppermost part of the LC layer (Fig. 4). The velocity at the top of the lower crust is estimated at 6.9 ± 0.4 km s^{-1}. The Moho is constrained by P_mP reflections (Figs. 4 and 6) at station 14 at a depth of about 14 km. This depth corresponds well with a cross-tie between lines LSSL2011-03/04 and TransArctic 1989–1991 (Fig. 7). Gravity modelling was used to define the Moho for the remainder of the profile. The Moho depth ranges from <30 km at Alpha Ridge to 14 km beneath Makarov Basin (Fig. 7). Interpretations of the MC and LC layers are discussed in Section 5.

4.4. Mantle

Seismic energy was not observed on any sonobuoy beyond an offset of 43 km; a limitation imposed by radiowave transmission of the received signal back to the ship and/or due to the seismic source energy. In comparison, along the ARTA line (Funck et al., 2011), the minimum offset for the mantle refraction P_n beneath Alpha Ridge is ~70 km. Along the TransArctic 1989–1991 profile, the P_n phase was observed at a minimum offset of 35 km in Makarov Basin (Lebedeva-Ivanova et al., 2011). No P_n phases were noticed in our sonobuoy data. As such, this study provides no information on upper mantle velocities.

5. Discussion

5.1. Sedimentary succession of Makarov Basin

The sedimentary history of Makarov Basin appears distinct from that of Canada Basin. Initial sediment input to Makarov Basin came from the Lomonosov Ridge/Barents Shelf (Evangelatos and Mosher, 2016), while in Canada Basin first sedimentary deposition on basement originated from the Alaskan margin (Mosher et al., 2012). After the separation and subsequent subsidence of Lomonosov Ridge from the Barents Shelf, topographic barriers (Alpha and Lomonosov ridges) hindered sedimentation into Makarov Basin from proximal sources. Consequently, mid-Upper Cretaceous to present sedimentary deposits in Makarov Basin are largely hemipelagic to pelagic (Evangelatos and Mosher, 2016), while turbidite deposition dominates in Canada Basin (Mosher et al., 2012).

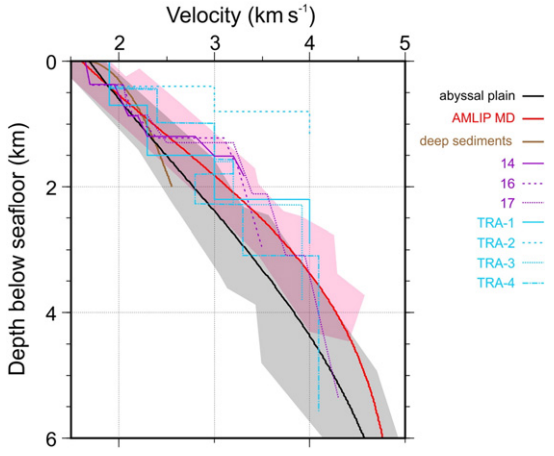

Fig. 9. Data from sonobuoys 14, 16 and 17, deployed in Makarov Basin, are plotted against regional velocity-depth curves calculated by Shimeld et al. (2016). The "abyssal plain" curve (black line) represents central Canada Basin, while the "AMLIP MD" curve (red line) is for sonobuoy locations enclosed by the area defined by the Alpha-Mendeleev LIP magnetic domain (Saltus et al., 2011; Fig. 2). The grey and pink shaded areas illustrate the range in data points (from Chian and Lebedeva-Ivanova [2015]) used to calculate the curves for the abyssal plain and AMLIP MD regions, respectively. The brown curve labelled "deep sediments" is a square root function derived from seismic refraction measurements made in deep-sea sediments (> ~3.6 km water-depth) from the Gulf of Mexico and North Atlantic (Nafe and Drake, 1961). TRA-1, -2, -3 and -4 are extracted from the velocity model of line TransArctic 1989–1991 (Lebedeva-Ivanova et al., 2011) at the points shown in Fig. 10. TRA-3 and TRA-4 were converted to the depth domain using interval velocities derived by Langinen et al. (2006).

Fig. 9 shows velocity-depth profiles of sedimentary layers from Makarov Basin plotted against the velocity-depth functions derived by Shimeld et al. (2016) for the Alpha-Mendeleev LIP magnetic domain and the abyssal plain of Canada Basin. In addition, a curve representing deep-sea sediments from the Gulf of Mexico and North Atlantic (Nafe and Drake, 1961) is also plotted in this figure. For depths of burial corresponding with layers S1–S3 (from 0 to ~1–1.3 km depth below seafloor; Fig. 9), velocities do not discriminate between the different functions. For the deeper succession (> ~1.3 km depth below seafloor), velocities from Makarov Basin best match the function for the Alpha-Mendeleev LIP magnetic domain (Fig. 9). This function is characterized by a high velocity gradient. Shimeld et al. (2016) argued that this trend cannot be readily explained by likely lithological variations and proposed enhanced chemical compaction due to "episodic high palaeo-heat flow" as an alternative. In their model, the anomalous heat flow values were caused by late magmatism related to the Alpha-Mendeleev LIP. The latest confirmed age of such magmatism is ~89 Ma, constrained by $^{40}Ar/^{39}Ar$ isotopic dating of basalt recovered in situ (Jokat et al., 2013). Assuming that its sedimentary succession consists of "siliciclastic sediments and sedimentary rocks" (Shimeld et al., 2016) typical of deep-water marine basins, this process could hypothetically explain the high velocities in Makarov Basin. Existing heat flow data is sparse and unevenly distributed (Fig. 2); hence, it cannot be used to validate the possibility that the deep succession was influenced by late magmatism. We thus prefer to attribute the high velocity of sedimentary layers to lithological factors including possible cementation/lithification. Volcanic or volcaniclastic material such as tuff that is cemented as part of its process of formation, intercalated with sediments, might also explain the higher than expected velocities. Such a relationship is suggested by high amplitude and semi-continuous reflections from these intervals (Evangelatos and Mosher, 2016; Fig. 8b). Volcanogenic material are plausibly related to mid-Late Cretaceous to Palaeocene volcanism on Ellesmere Island and northern Greenland (Estrada et al., 2010; Tegner et al., 2011). Diagenetic biosiliceous units may be a contributing factor. Biosiliceous ooze was identified in dredge samples from Alpha Ridge (CESAR; Mudie and Blasco, 1985) and in core from Lomonosov Ridge (IODP 302; Backman et al., 2006, 2008).

5.2. Crust of Alpha Ridge

In our study, the velocity of the uppermost volcanic crust ranges from 3.3 to 3.6 km s^{-1}. The location and results from other studies are shown in Figs. 10 and 11, respectively. Funck et al. (2011) reported velocities of up to 4.7 km s^{-1}, while Bruvoll et al. (2012) showed it to be as low as 3.0 km s^{-1}. Two possibilities are offered to explain the variation in velocities for the uppermost crust shown in Fig. 11:

1) The resolution of the various data sets is different depending on acquisition parameters, processing and data quality. For example, a velocity layer similar to UC1 was not identified in the ARTA experiment (Funck et al., 2011; Fig. 11), yet the seismic reflection data from their study show intra-basement acoustic facies similar to that described here for UC1. We assume that a layer similar to UC1 is unresolved in the ARTA experiment due to the difference in seismic trace spacing between our study (20–30 m; Mosher, 2012) vs. ARTA (1200–1500 m; Funck et al., 2011). For the Polarstern 1998 (Jokat, 2003)

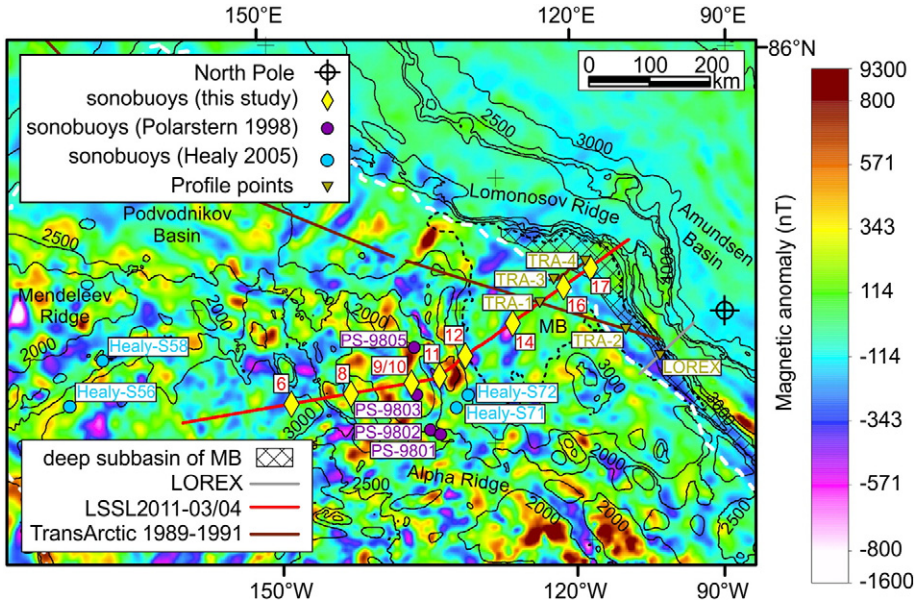

Fig. 10. Colour-shaded magnetic map of northern Amerasia and Eurasia basins. Makarov Basin is delineated by a dashed black line representing the 3700 m bathymetric contour. Thin black lines are bathymetric contours for 1000, 2000, 2500, 3000 and 4000 m. The white dashed line delineates the Alpha-Mendeleev LIP magnetic domain (Saltus et al., 2011). Other studies shown in this figure are: sonobuoys from Healy 2005 (Bruvoll et al., 2012), sonobuoys from Polarstern 1998 (Jokat, 2003), LOREX (dip line) (Forsyth and Mair, 1984), the TransArctic 1989–1991 line (Lebedeva-Ivanova et al., 2011) and the deep subbasin of MB (Makarov Basin) (Evangelatos and Mosher, 2016). The magnetic compilation is from Gaina et al. (2011) and the isobaths were produced using the IBCAO compilation (Jakobsson et al., 2012). Values above 800 nT and below −800 nT are saturated.

and Healy 2005 experiments (Bruvoll et al., 2012) (Fig. 11), modelling did not resolve crustal velocity structures below shallow basement as seismic energy was generally only recorded to offsets <15 km.

2) Variation in seismic velocities may reflect lithological heterogeneity in the composition of shallow basement. Seismic patterns and facies in layer UC1 resemble basement as identified by Jokat (2003) and Bruvoll et al. (2012) in their respective studies of seismic reflection profiles over the Alpha-Mendeleev ridge complex. Jokat (2003) reported that a basaltic fragment recovered at the base of a sediment core (Jokat, 1999) is representative of basement. Dredging on the Canada Basin-facing flank of Alpha Ridge recovered tuff (Mayer et al., 2016). Bruvoll et al. (2012) interpreted basement at the Alpha-Mendeleev ridge complex as composed of massive lava flows, tuff and pillow basalts. They attributed the presence of relatively low P-wave velocities to intercalated sedimentary rock between volcanic beds. Intra-basement seismic facies and P-wave velocities from the Alpha and Mendeleev ridges (Jokat, 2003; Bruvoll et al., 2012; this study) resemble results from Manihiki Plateau (Pietsch and Uenzelmann-Neben, 2015). Hochmuth (2015) assigned P-wave velocities as low as 3.0 to 4.3 km s^{-1} for the upper crust at the western part of Manihiki Plateau. At the eastern part of this feature, basalts, intercepted near the top of basement in drill core (DSDP Leg 33 Site 317; Schlanger et al., 1976), correspond with interval velocities of 3.5–4.0 s^{-1} (Pietsch and Uenzelmann-Neben, 2015).

The MCS record mostly shows incoherent noise in layer UC2 (Fig. 8). Based on previous studies, Alpha Ridge formed or was significantly altered as a result of a LIP. The upper crust of Alpha Ridge is, therefore, interpreted as a magmatic succession with a combined average thickness of 3.2 km and a velocity range of 3.3–5.6 km s^{-1} (Fig. 5). The thick successions of basalt at the Faroe Islands, at least 6.6 km (Passey and Bell, 2007), present a plausible analogue to the magmatic upper crust of Alpha Ridge. Along line Arctic-2000 (Fig. 12), Lebedeva-Ivanova et al. (2006) interpreted layers with P-wave velocities of 5.0–5.4 km s^{-1} (their layer *IV*) as "dominated by carbonate and terrigenous sedimentary rocks, with some igneous intercalations". This interpretation is based on the assumption that recovered dredge samples of such rock types in the vicinity of the line are in situ (Kaban'kov et al., 2004). Coincident seismic reflection data are available; however, layer *IV* is inadequately resolved (Lebedeva-Ivanova et al., 2006). During the more recent Arctic-2012 expedition, a mix of carbonate (dominant), terrigenous, metamorphic and igneous rock types were recovered along steep slopes of the Mendeleev Ridge (Morozov et al., 2013; Gusev et al., 2014), which Petrov et al. (2016) interpreted as evidence in support of the continental affinity of this ridge. Assuming that Alpha and Mendeleev ridges represent a single geological entity, as suggested by studies of potential fields and seismic refraction modelling (e.g., Dove et al., 2010; Funck et al., 2011), then layer *IV* in the model of Lebedeva-Ivanova et al. (2006) and our layer UC3 are stratigraphically equivalent. We question, however, the interpretation of these layers as chiefly sedimentary. Shallow drilling (<2 m) through basement confirmed only the presence of basalt from Mendeleev Ridge (Petrov et al., 2016). With respect to this study, the MCS data do not show seismic facies consistent with carbonates or terrigenous sedimentary rock (e.g., stratification, progradation structures, carbonate platforms), but imaging is admittedly limited at these depths.

Velocities for the MC layer (6.0–6.5 km s^{-1}) are fast relative to fresh basalts. Grevemeyer et al. (1998) modelled layer 2A oceanic crust using P-wave velocities of 2.9–4.3 km s^{-1} and Bourbié et al. (1987) lists the maximum value for basalt at 6 km s^{-1}. The velocities for the MC layer are also slower than those reported for mid-crustal gabbros (6.95 ± 0.22 km s^{-1}; Holbrook et al., 1992). Such intermediate values (6.0–6.5 km s^{-1}) are more consistent with metabasalts and metadolerites (≤6.25 km s^{-1}) measured from rock samples from the Bay of Islands ophiolite complex in Newfoundland, Canada (Salisbury and Christensen, 1978). These lithologies represent the sheeted dykes that define oceanic layer 2C (Becker et al., 1989; Carlson and Herrick, 1990), where velocities of 5.8–6.5 km s^{-1} are reported (Ewing, 1976). Alternatively, Lebedeva-Ivanova et al. (2006), who favoured a continental origin for Mendeleev Ridge, interpreted their layer *V* (5.9–6.5 km s^{-1}) as magmatically altered crystalline basement. Their interpretation is based on correlations with the TransArctic 1989–1991 line and similarities to velocities derived from outcropping granite at Henrietta Island on the Siberian Shelf. If the continental model is correct,

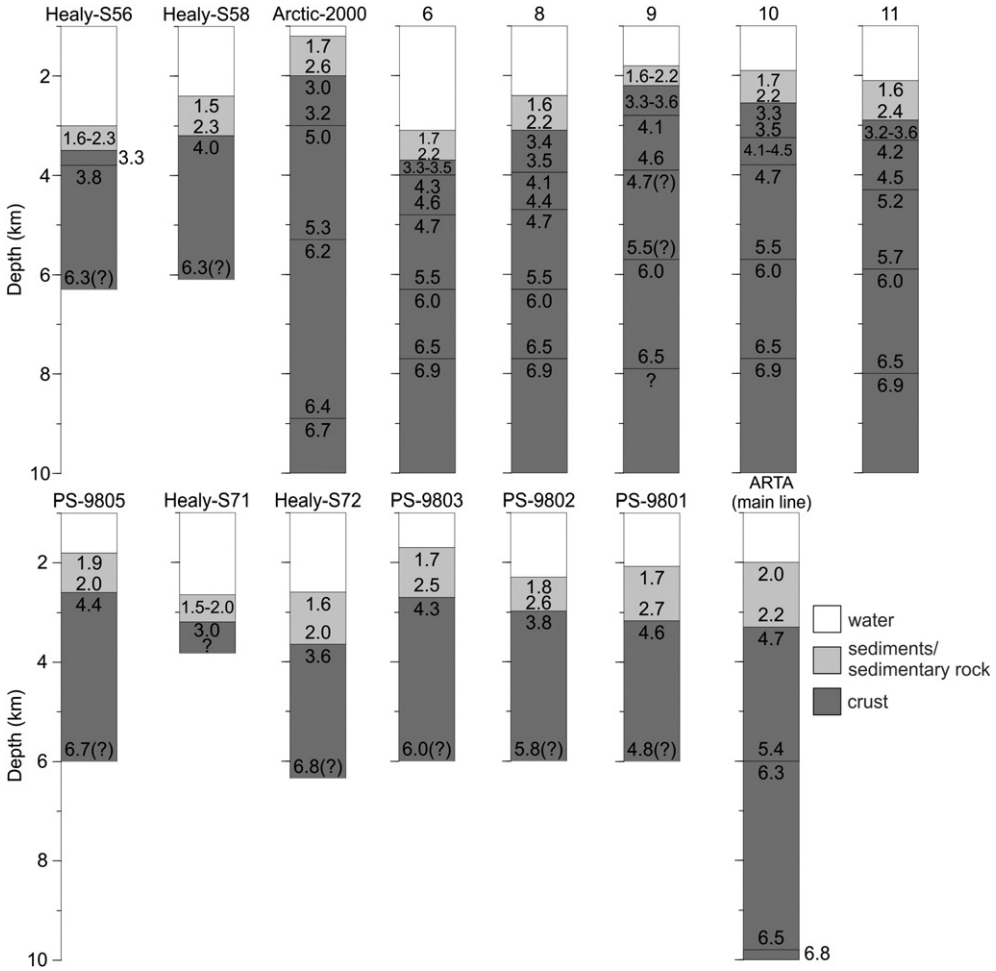

Fig. 11. Comparison of P-wave velocities from this study with other experiments from the Alpha and Mendeleev ridges. ARTA (main line) is from Funck et al. (2011), Arctic-2000 is from Lebedeva-Ivanova et al. (2006), Healy-S56, -S58, -S71, -S72 are from Bruvoll et al. (2012), PS-9801, -9802, -9803, -9805 are from Jokat (2003), and labels 6, 8, 9, 10 and 11 are stations from this study. Velocities for the Arctic-2000 and ARTA columns are extracted from 265 km and 80 km distance along their respective lines (Fig. 1). Note, we re-interpret layers *III* (3.0–3.2 km s^{-1}) and *IV* (5.0–5.3 km s^{-1}) from Arctic-2000 as part of the crust (refer to Section 5.2). Velocities are specified in km s^{-1}.

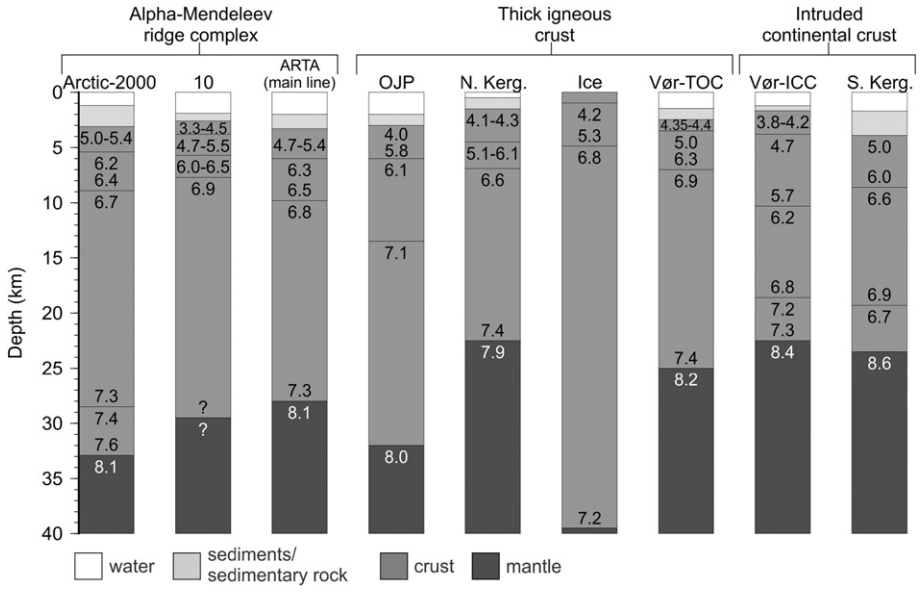

Fig. 12. Comparison of P-wave velocities from the Alpha-Mendeleev ridge complex with other LIPs. Vertical profiles extracted for Mendeleev Ridge: Arctic-2000 (Lebedeva-Ivanova et al., 2006); Alpha Ridge: ARTA (main line) (Funck et al., 2011) and station 10 (this study); Ontong Java Plateau: OJP (Gladczenko et al., 1997), Iceland: Ice (Darbyshire et al., 1998), North and South Kerguelen Plateau: N. Kerg. (Charvis et al., 1995) and S. Kerg. (Operto and Charvis, 1995), respectively; Thick Oceanic Crust and Intruded Continental Crust of Vøring Marign: Vør-TOC and Vør-ICC (Mjelde et al., 2005), respectively. Velocities are specified in km s^{-1}. For station 10, Moho depth is based on gravity modelling (refer to Section 3.3.3).

the Alpha-Mendeleev ridge complex is similar to the southern Kerguelen Plateau, which is inferred to represent stretched continental crust overprinted by plume-related magmatism (Operto and Charvis, 1995).

The thickness of the LC layer is based on gravity modelling calibrated at a single station (Fig. 6). Despite this limitation, even by the most conservative estimate, the lower crust constitutes a large fraction of the total crustal thickness of Alpha Ridge (Fig. 12). The thickness of the lower crust, and overall crustal thickness (25–30 km; Fig. 12), is consistent along the length of Alpha and Mendeleev ridges (Lebedeva-Ivanova et al., 2006; Funck et al., 2011; this study). It should be noted, however, that deep seismic studies of Alpha and Mendeleev ridges are few relative to the size of the ridge complex. As such, the apparently homogeneous structure of those ridges may be due to aliasing and/or data resolution.

In summary, the internal crustal velocity structure of Alpha Ridge consists of a 2.3–4.5 km-thick succession of magmatic rock (chiefly extrusive rock) lying above a 1.4–2.1 km thick middle layer with intermediate velocities (6.0–6.5 km s^{-1}) that, in turn, overlies a relatively thick lower crust with high velocities (> 6.9 km s^{-1}). Together with the basement pattern from the MCS data and its magnetic character, Alpha Ridge is consistent with other LIPs with thick igneous crust (Fig. 12). This velocity structure differs from magmatically overprinted thinned continental crust (e.g., intruded continental crust on the Vøring margin; Mjelde et al., 2005) (Fig. 12). This interpretation suggests that the Alpha-Mendeleev ridge complex initially formed as an Iceland-type structure during seafloor spreading in Amerasia Basin (Vogt et al., 1979; Forsyth et al., 1986; Jackson et al., 1986; Asudeh et al., 1988; Weber, 1990; Lane, 1997); or at a later stage in the history of the basin (Grantz et al., 2011). With respect to an Iceland-type model, Brumley (2009) argued that the stress field implied by the extinct spreading centre in Canada Basin (Fig. 2) is inconsistent with the general orientation of rift structures (troughs and ridges) on the Alpha-Mendeleev ridge complex (Fig. 1). Aside from discriminating large-scale crustal types based on velocity structure, the seismic and gravity data cannot resolve possible continental fragments entrained within predominantly magmatic crust or if magma intruded original continental material.

5.3. Crust of Makarov Basin

Based on their interpretation of the TransArctic 1989–1991 seismic refraction data, Lebedeva-Ivanova et al. (2011) concluded that Makarov Basin was probably underlain by oceanic crust, except for continental fragments or slivers that rifted off Lomonosov Ridge (e.g., Marvin Spur; Fig. 1). Models of the crustal velocity structure for Makarov Basin differ between this study and the TransArctic 1989–1991 profile (Fig. 13). Discrepancies are attributed to resolution of the data sets. Specifically, the TransArctic 1989–1991 experiment involved a receiver spacing of 7–14 km (Lebedeva-Ivanova et al., 2011). Consequently, some of the layer boundaries for the upper and mid-crustal layers for the TransArctic 1989–1991 line are modelled based on only a few seismic traces and, therefore, are not well constrained. In comparison, the seismic trace spacing for our experiment was 20–30 m (Mosher, 2012), thereby resulting in denser ray coverage in the vicinity of the sonobuoy stations.

In Makarov Basin, between 360 and 560 km along line (Fig. 5), velocities for layers UC2, UC3 and MC are similar or slightly faster relative to layers from Alpha Ridge. We propose that the absence of significant lateral variations in velocity structure between Alpha Ridge and part of Makarov Basin (from 360 to 560 km; Fig. 5) is due to lithological homogeneity. If the Alpha-Mendeleev LIP was emplaced late in the history of Amerasia Basin, lithological homogeneity results from significant magmatic overprinting of the crust of Makarov Basin. A large part of Makarov Basin closest to Alpha Ridge is, indeed, included within the Alpha-Mendeleev LIP magnetic domain (Saltus et al., 2011; Oakey and Saltus, 2016; Figs. 2 and 10), which corroborates this tectonic model. The change in crustal thickness from the foot of Alpha Ridge to central Makarov Basin (360 km to 560 km along line; Fig. 7) is gradual, thinning from 10 km to 8–9 km over a distance of 200 km. Such a relationship is noted between the Manihiki Plateau and the adjacent Samoan Basin (Hochmuth, 2015). Passive rift margins may also exhibit gradual transitions from shallow shelves to deep basins, but lateral changes in velocity structure are much more apparent in such cases (e.g., southeast Greenland margin; Korenaga et al., 2000). The tectonic model of Grantz et al. (2011) shows Makarov Basin forming during the initial phases of opening of Amerasia Basin. According to this model, the Alpha-Mendeleev ridge complex was emplaced later on oceanic crust. Velocity-depth profiles indicate that crustal layers for Makarov Basin are generally thick relative to normal oceanic crust of comparable age (Fig. 14). Assuming

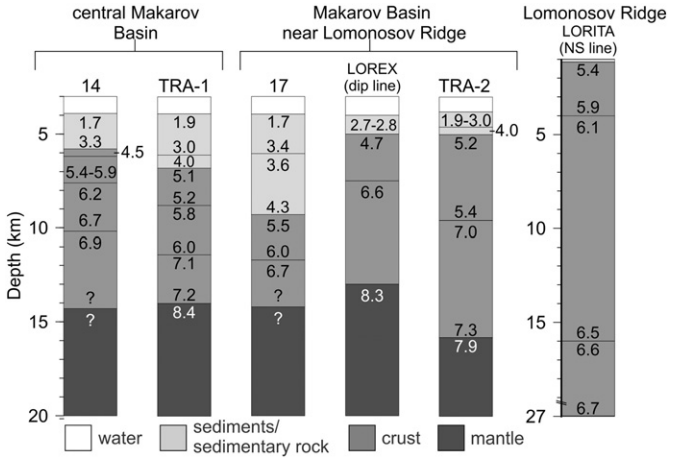

Fig. 13. Comparison of P-wave velocities from this study with other experiments from Makarov Basin. LOREX (dip line) is from Forsyth and Mair (1984), LORITA (NS line) is from Jackson et al. (2010), TRA-1 and TRA-2 are extracted along line TransArctic 1989–1991 from Lebedeva-Ivanova et al. (2011), and stations 14 and 17 are from this study (locations shown in Fig. 10). Velocities are specified in km s^{-1}. For stations 14 and 17, Moho depth is based on gravity modelling (refer to Section 3.3.3).

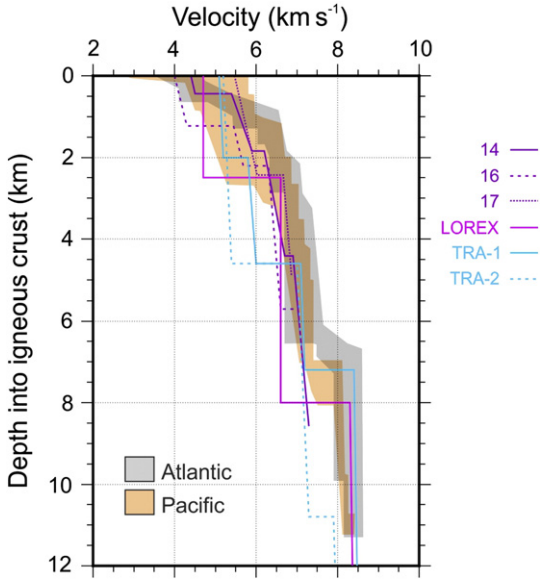

Fig. 14. P-wave velocity profiles of stations 14, 16 and 17 (this study), LOREX (dip line) (Forsyth and Mair, 1984), and TRA-1 and TRA-2 are extracted along line TransArctic 1989–1991 (Lebedeva-Ivanova et al., 2011). Locations are shown in Fig. 10. Grey and orange shaded areas illustrate the range in data points for normal oceanic crust from the Atlantic (59–127 Ma) and Pacific (29–140 Ma) oceans (White et al., 1992), respectively.

that the crust is oceanic in origin, thickening is attributed to magmatism related to the Alpha-Mendeleev LIP. Alternatively, the LIP extruded through and on top of stretched continental crust, as Chian et al. (2016) described extensive regions of stretched continental crust within Canada Basin. Døssing et al. (2013) proposed that linear magnetic anomalies close to the Canadian Arctic margin (Fig. 1) are caused by a Upper Jurassic–Lower Cretaceous dyke swarm related to initial rifting of the Amerasia Basin. Assuming this rift zone extends farther west and away from the Canadian Arctic margin, the implication is that the crust of Makarov Basin is continental in origin. The general orientation of the stress field responsible for the dyke swarm, however, is at odds with the observed extensional fabric of Alpha Ridge (Fig. 1).

The top of a basement structure at 550–570 km along line (Fig. 8b) is resolved by the MCS data. The velocity structure of this feature (6.2–6.6 km s^{-1}) is constrained by the $P_{mc}P$ phase (Figs. 4 and 5). Evangelatos and Mosher (2016) suggested that this structure splayed off of Lomonosov Ridge as a result of transtension, similar to Marvin Spur (Cochran et al., 2006). As shown in Fig. 7, the lack of a corresponding magnetic response, as one would expect if this feature was magmatic, supports a continental origin for this structure. The TransArctic 1989–1991 line resolves a similar basement structure between Marvin Spur and Lomonosov Ridge (Lebedeva-Ivanova et al., 2011; TRA-2 in Fig. 10). Modelled velocities for this feature resemble upper crustal velocities (5.8–6.5 km s^{-1}) from the LORITA line on Lomonosov Ridge (Jackson et al., 2010; refer to Fig. 1 for location).

In the deep subbasin of Makarov Basin, bounded by Lomonosov Ridge and the pronounced basement structure at 550–570 km along line (Fig. 8b), there is disagreement in velocity structure between station 17, the TransArctic 1989–1991 profile and the LOREX line (Fig. 13). Again, the deviations are attributed to differences in resolution due to inconsistent acquisition methods. Morphological evidence (horsetail splays and a rhomboid shape) suggests that the subbasin is a pull-apart basin formed by transtension (Evangelatos and Mosher, 2016). If this interpretation is correct, the narrow width of the subbasin (Figs. 2 and 10) favours highly stretched continental crust beneath this part of Makarov Basin. Assuming a genetic tie between the subbasin and the Lomonosov Ridge, velocities for layer UC3 (5.4–6.0 km s^{-1}) are plausibly equivalent to pre-Cenozoic (meta-)sedimentary rock from the ridge where P-wave velocities of ~3.7–5.9 km s^{-1} (Jokat, 2005) and 5.4–5.9 km s^{-1} (Jackson et al., 2010) are reported. Alternatively, the subbasin may be underlain by oceanic crust, as proposed by Forsyth and Mair (1984) for the LOREX line. As shown in Fig. 14, velocities for station 17 are compatible with normal oceanic crust; however, results from LOREX and the TransArctic 1989–1991 line (TRA-2) are less consistent.

In contrast to the gradual transition between Alpha Ridge and Makarov Basin, the crust thins over a lateral distance of 70 km from 20 km at Lomonosov Ridge to 5 km in Makarov Basin (Fig. 7). This abrupt transition is also noted in the LOREX line (Forsyth and Mair, 1984) and is consistent with crustal studies at transform margins (e.g., southwest Newfoundland margin; Todd et al., 1988). This interpretation corroborates previous work that concluded that the Makarov Basin-facing side of Lomonosov Ridge is part of a strike-slip system (e.g., Cochran et al., 2006; Evangelatos and Mosher, 2016). Lateral changes in lower crustal velocities are also more apparent from Makarov Basin to Lomonosov Ridge (Fig. 13) compared to the transition from Alpha Ridge to Makarov Basin (Fig. 5). The properties of the LC layer are, however, principally constrained by gravity modelling.

6. Conclusions

From a geological perspective, the northern Amerasia Basin in the Arctic Ocean is amongst the least understood regions on Earth. To gain insight on the tectonic history of this region, nine seismic records from sonobuoys spanning almost 650 km from Alpha Ridge and across Makarov Basin to Lomonosov Ridge were analyzed. Velocities from the upper sedimentary layers of Makarov Basin do not deviate significantly from velocity-depth curves for typical siliciclastic deep-sea sediments. Deeper sedimentary layers have velocities that are similar to those of equivalent burial depth found within the Alpha-Mendeleev LIP magnetic domain in northern Canada Basin. We attribute the high velocities of this section to interbedded volcanic/volcaniclastic rock. Biosiliceous sediments may have also contributed to the high velocities.

The shallow part of the upper crust for Alpha Ridge and part of Makarov Basin (360 to 560 km along line; Fig. 5) is interpreted as volcaniclastic/volcanic rock, possibly intercalated with minor sedimentary rock. Overall, however, the upper crust of Alpha Ridge is a thick succession (2.5–3.5 km) of magmatic (primarily extrusive) rock. The mid-crustal layer is 1.4–2.1 km thick with velocities intermediate between those of fresh basalts and gabbro. Gravity modelling suggests that the lower crust constitutes more than half of the total thickness of the crust beneath Alpha Ridge. These characteristics of the crustal structure of Alpha Ridge are consistent with a tectonic and magmatic origin similar to other LIPs with thick igneous crust. The presence of continental crust in Alpha Ridge, however, cannot be ruled out.

The crustal velocity structure of Alpha Ridge and Makarov Basin (between 360 and 560 km distance) is similar with deviations <0.3 km s^{-1} (Fig. 5), which is within the uncertainties of the velocity model. The implication is that these two features share a common geological origin, or that the emplacement of Alpha-Mendeleev LIP modified the crust of Makarov Basin to such extent that it resembles a condensed version of the crust of Alpha Ridge. Crustal thickening towards Alpha Ridge is also attributed to the emplacement of the LIP.

The results from density modelling suggest that the transition from Lomonosov Ridge to Makarov Basin is characterized by a 15 km decrease in crustal thickness over a distance of only 70 km. Such a sharp transition is consistent with past interpretations of the Amerasian flank of Lomonosov Ridge as a transform/transtensional margin. A non-magnetic basement structure in Makarov Basin, previously interpreted as a splay structure related to transtension, is genetically tied to the upper crust of Lomonosov Ridge by similarities in seismic velocity structure.

Acknowledgements

The authors would like to express their appreciation to the officers, crew and scientific staff of the Canadian icebreaker CCGS Louis S. St-Laurent and the US icebreaker USCGC Healy, as well as the Canadian and US Extended Continental Shelf mapping programs. Processing of the data benefited from guidance and discussions with D. Chian. J. Shimeld is acknowledged for processing the seismic reflection data, and B. Coakley for processing the gravity data.

This manuscript is part of the doctoral thesis of JE. This project is supported financially by a Natural Sciences and Engineering Research Council (NSERC) of Canada graduate scholarship, NSERC Discovery Grant RGPIN 314089 to DCM, and by in-kind contributions by the Geological Survey of Canada (GSC). Funding to JE for a three-month visit to GEUS in 2013 was provided by the NSERC's Michael Smith Foreign Study Supplements and a research grant from the Geological Society of America. JE is grateful for the hospitality and support provided by GEUS during the visit. We thank S. Dehler, G. Oakey, B. Coakley and W. Jokat for their comprehensive reviews.

References

Andronikov, A., Mukasa, S., Mayer, L.A., Brumley, K., 2008. First recovery of submarine basalts from the Chukchi Borderland and Alpha/Mendeleev Ridge, Arctic Ocean. Eos 89 (5) (Abstract V41D–2124).

Asudeh, I., Green, A.G., Forsyth, D.A., 1988. Canadian expedition to study the Alpha-Ridge complex — results of the seismic refraction survey. Geophys. J. 92, 283–301.

Backman, J., Moran, K., McInroy, D.B., Mayer, L.A., 2006. Expedition 302 scientists. Proc. Integr. Ocean Drill Program 302. http://dx.doi.org/10.2204/iodp.proc.302.101.2006.

Backman, J., Jakobsson, M., Frank, M., Sangiorgi, F., Brinkhuis, H., et al., 2008. Age model and core-seismic integration for the Cenozoic Arctic Coring Expedition sediments

from the Lomonosov Ridge. Paleoceanography 23 (PA1S03). http://dx.doi.org/10.1029/2007PA001476.
Becker, K., Sakai, H., et al., 1989. Drilling deep into young oceanic crust, Hole 504B, Costa Rica Rift. Rev. Geophys. 27, 79–102.
Bourbié, T., Coussy, O., Zinszner, B., 1987. Acoustics of Porous Media. Ed. Technip (334 pp.).
Brozena, J.M., Childers, V.A., Lawver, L.A., Gahagan, L.M., Forsberg, R., Faleide, J.I., Eldholm, O., 2003. New aerogeophysical study of the Eurasia Basin and Lomonosov Ridge: implications for basin development. Geology 31, 825–828.
Brumley, K., 2009. Tectonic Geomorphology of the Chukchi Borderland: Constraint for Tectonic Reconstruction Models. M.Sc. Thesis, University of Alaska, Fairbanks (116 pp.), (unpublished).
Bruvoll, V., Kristoffersen, Y., Coakley, B.J., Hopper, J.R., 2010. Hemipelagic deposits on the Mendeleev and northwestern Alpha submarine ridges in the Arctic Ocean: acoustic stratigraphy, depositional environment and an inter-ridge correlation calibrated by the ACEX results. Mar. Geophys. Res. 31, 149–171.
Bruvoll, V., Kristoffersen, Y., Coakley, B.J., Hopper, J.R., Planke, S., Kandilarov, A., 2012. The nature of the acoustic basement on Mendeleev and northwestern Alpha ridges, Arctic Ocean. Tectonophysics 514, 123–145.
Buchan, K.L., Ernst, R., 2006. Giant dyke swarms and the reconstruction of the Canadian Arctic islands, Greenland, Svalbard and Franz Josef Land. In: Hanski, E., Mertanen, S., Ramo, T., Vuollo, J. (Eds.), Dyke Swarms: Time Markers of Crustal Evolution. Taylor & Francis, London, pp. 27–48.
Carlson, R.L., Herrick, C.N., 1990. Densities and porosities in the oceanic crust and their variations with depth and age. J. Geophys. Res. 95, 9153–9170.
Charvis, P., Recq, M., Operto, S., Brefort, D., 1995. Deep structure of the northern Kerguelen Plateau and hotspot-related activity. Geophys. J. Int. 122, 899–924.
Chian, D., Lebedeva-Ivanova, N.N., 2015. Atlas of sonobuoy velocity analyses. Canada Basin, Geological Survey of Canada, Open File 7661 (55 pp.). 10.4095/295857.
Chian, D., Jackson, H.R., Hutchinson, D.R., Shimeld, J.W., Oakey, G.N., Lebedeva-Ivanova, N., Li, Q., Saltus, R.W., Mosher, D.C., 2016. Distribution of crustal types in Canada Basin, Arctic Ocean. Tectonophysics 691:8–30 http://dx.doi.org/10.1016/j.tecto.2016.01.038.
Coakley, B.J., Cochran, J.R., 1998. Gravity evidence of very thin crust at the Gakkel Ridge (Arctic Ocean). Earth Planet. Sci. Lett. 162, 81–95.
Cochran, J.R., Edwards, M.H., Coakley, B.J., 2006. Morphology and structure of the Lomonosov Ridge, Arctic Ocean. Geochem. Geophys. Geosyst. 7:Q05019. http://dx.doi.org/10.1029/2005GC001114.
Darbyshire, F.A., Bjarnason, I.T., White, R.S., Flóvenz, Ó.G., 1998. Crustal structure above the Iceland mantle plume imaged by the ICEMELT refraction profile. Geophys. J. Int. 135, 1131–1149.
Doré, A.G., Lundin, E.R., Gibbons, A., Sømme, T.O., Tørudbakken, B.O., 2015. Transform margins of the Arctic: a synthesis and re-evaluation. In: Nemčok, M., Rybár, S., Sinha, S.T., Hermeston, S.A., Ledvényiová, L. (Eds.), Transform Margins: Development, Controls and Petroleum Systems. Geol. Soc. London, Special Publications 431. http://dx.doi.org/10.1144/SP431.8.
Døssing, A., Jackson, H.R., Matzka, J., Einarsson, I., Rasmussen, T.M., Olesen, A.V., Brozena, J.M., 2013. On the origin of the Amerasia Basin and the high Arctic large igneous province – results of new aeromagnetic data. Earth Planet. Sci. Lett. 363, 219–230.
Døssing, A., Hansen, T.M., Olesen, A.V., Hopper, J.R., Funck, T., 2014. Gravity inversion predicts the nature of the Amundsen basin and its continental borderlands near Greenland. Earth Planet. Sci. Lett. 408:132–145. http://dx.doi.org/10.1016/j.epsl.2014.10.011.
Dove, D., Coakley, B., Hopper, J., Kristoffersen, Y., the HLY0503 Geophysics Team, 2010. Bathymetry, controlled source seismic and gravity observations of the Mendeleev ridge: implications for ridge structure, origin, and regional tectonics. Geophys. J. Int. 183: 481–502. http://dx.doi.org/10.1111/j.1365-246X.2010.04746.x.
Embry, A.F., Osadetz, K.G., 1988. Stratigraphy and tectonic significance of Cretaceous volcanism in the Queen Elizabeth Islands, Canadian Arctic Archipelago. Can. J. Earth Sci. 25, 1209–1219.
Estrada, S., 2015. Geochemical and Sr–Nd isotope variations within Cretaceous continental flood-basalt suites of the Canadian High Arctic with a focus on the Hassel Formation basalts of northeast Ellesmere Island. Int. J. Earth Sci. 104, 1981–2005.
Estrada, S., Henjes-Kunst, F., Melcher, F., Tessensohn, F., 2010. Paleocene alkaline volcanism in the Nares Strait region: evidence from volcanic pebbles. Int. J. Earth Sci. 99, 863–890.
Evangelatos, J., Mosher, D.C., 2016. Seismic stratigraphy, structure and morphology of Makarov Basin: tectonic implications. Mar. Geol. 374, 1–13.
Forsyth, D.A., Mair, J.A., 1984. Crustal structure of the Lomonosov Ridge and the Fram and Makarov Basins near the North Pole. J. Geophys. Res. 89 (B1), 473–481.
Forsyth, D.A., Asudeh, I., Green, A.G., Jackson, H.R., 1986. Crustal structure of the northern Alpha Ridge beneath the Arctic Ocean. Nature 322, 349–352.
Funck, T., Jackson, H.R., Shimeld, J., 2011. The crustal structure of the Alpha Ridge at the transition to the Canadian Polar Margin: results from a seismic refraction experiment. J. Geophys. Res. 116:B12101. http://dx.doi.org/10.1029/2011JB008411.
Gaina, C., Werner, S.C., Saltus, R., Maus, S., 2011. Circum-Arctic mapping project: new magnetic and gravity anomaly maps of the Arctic. In: Spencer, A.M., Embry, A.F., Gautier, D.L., Stoupakova, A.V., Sørensen, K. (Eds.), Arctic Petroleum Geology: Geol. Soc. London, Memoirs 35, pp. 39–48.
Gladczenko, T.P., Coffin, M.F., Eldholm, O., 1997. Crustal structure of the Ontong Java Plateau: modeling of new gravity and existing seismic data. J. Geophys. Res. 102, 22711–22729.
Grantz, A., Eittreim, S., Dinter, D.A., 1979. Geology and tectonic development of the continental margin north of Alaska. Tectonophysics 59, 263–291.
Grantz, A., Clark, D.L., Phillips, R.L., Srivastava, S.P., Blome, C.D., Gray, L.B., Haga, H., Mamet, B.L., McIntyre, D.J., Mcneil, D.H., Mickey, M.B., Mullen, M.W., Murchey, B.I., Ross, C.A., Stevens, C.H., Silberling, N.J., Wall, J.H., Willard, D.A., 1998. Phanerozoic stratigraphy of Northwind Ridge, magnetic anomalies in the Canada basin, and the geometry and timing of rifting in the Amerasia basin, Arctic Ocean. GSA Bull. 110, 801–820.
Grantz, A., Hart, P.E., Childers, V.A., 2011. Geology and tectonic development of the Amerasia and Canada Basins, Arctic Ocean. In: Spencer, A.M., Embry, A.F., Gautier, D.L., Stoupakova, A.V., Sørensen, K. (Eds.), Arctic Petroleum Geology: Geol. Soc. London, Memoirs 35, pp. 771–799.
Grevemeyer, I., Weigel, W., Jennrich, C., 1998. Structure and ageing of oceanic crust at 14°S on the East Pacific Rise. Geophys. J. Int. 135, 573–584.
Gusev, E.A., Lukashenko, R.V., Popko, A.O., Rekant, P.V., Mirolyubova, E.S., Pyatkova, M.N., 2014. New data on the structure of slopes of the Mendeleev ridge seamounts (Arctic Ocean). Dokl. Earth Sci. 455, 250–253.
Hochmuth, K., 2015. From Crustal Structure to Plate Kinematics - The Role of Large Igneous Provinces in the Pacific Ocean. (PhD thesis). Universität Bremen, Bremen (176 pp.).
Holbrook, W.S., Mooney, W.D., Christensen, N.I., 1992. The seismic velocity structure of the deep continental crust. In: Fountain, D.M., Arculus, R., Kay, R.W. (Eds.), Continental Lower Crust, Developments in Geotectonics 23. Elsevier, New York, pp. 1–42.
Houtz, R., Ewing, J., 1976. Upper crustal structure as a function of plate age. J. Geophys. Res. 81, 2490–2498.
Hunt, C., Moskowitz, B.M., Banerjee, S.K., 1995. Magnetic properties of rocks and minerals. In: Ahrens, T.J. (Ed.), Rock Physics and Phase Relations: A Handbook of Physical Constants. American Geophysical Union.
Jackson, H.R., Mudie, P.J., Blasco, S.M. (Eds.), 1985. Initial geological report on CESAR-the Canadian expedition to study the Alpha Ridge, Arctic Ocean. Geol. Surv. Can. Pap. 84-22 (177 pp).
Jackson, H.R., Forsyth, D.A., Johnson, G.L., 1986. Oceanic affinities of the Alpha Ridge, Arctic Ocean. Mar. Geol. 73, 237–261.
Jackson, H.R., Dahl-Jensen, T., the LORITA Working Group, 2010. Sedimentary and crustal structure from the Ellesmere Island and Greenland continental shelves onto the Lomonosov Ridge, Arctic Ocean. Geophys. J. Int. 182:11–35. http://dx.doi.org/10.1111/j.1365-246X.2010.04604.x.
Jakobsson, M., Mayer, L., Coakley, B., Dowdeswell, J.A., Forbes, S., et al., 2012. The international Bathymetric Chart of the Arctic Ocean (IBCAO) version 3.0. Geophys. Res. Lett. 39:L12609. http://dx.doi.org/10.1029/2012GL052219.
Johnson, L., Grantz, A., Weber, J.R., 1990. Bathymetry and physiography. In: Grantz, A., Johnson, L., Sweeney, J. (Eds.), The Geology of North America, The Arctic Ocean Region vol. L. The Geological Society of America, pp. 63–75.
Jokat, W. (Ed.), 1999. ARCTIC '98: the expedition ARK-XIV 1a of RV "Polarstern" in 1998Berichte Zur Polarforschung 308. AWI, Bremerhaven (159 pp.).
Jokat, W., 2003. Seismic investigations along the western sector of Alpha Ridge, Central Arctic Ocean. Geophys. J. Int. 152, 185–201.
Jokat, W., 2005. The sedimentary structure of the Lomonosov Ridge between 88°N and 80°N. Geophys. J. Int. 163, 698–726.
Jokat, W., Ickrath, M., 2015. Structure of ridges and basins off East Siberia along 81 degrees N, Arctic Ocean. Mar. Petrol. Geol. 64, 222–232.
Jokat, W., Schmidt-Aursch, M.C., 2007. Geophysical characteristics of the ultra-slow spreading Gakkel ridge, Arctic Ocean. Geophys. J. Int. 168, 983–998.
Jokat, W., Uenzelmann-Neben, G., Kristoffersen, Y., Rasmussen, T., 1992. ARCTIC'91: Lomonosov Ridge—a double sided continental margin. Geology 20, 887–890.
Jokat, W., Weigelt, E., Kristoffersen, Y., Rasmussen, T., Schöne, T., 1995. New insights into the evolution of the Lomonosov Ridge and the Eurasian Basin. Geophys. J. Int. 122, 378–392.
Jokat, W., Ickrath, M., O'Connor, J., 2013. Seismic transect across the Lomonosov and Mendeleev Ridges: constraints on the geological evolution of the Amerasia Basin, Arctic Ocean. Geophys. Res. Lett. 40, 5047–5051.
Kaban'kov, V.Y., Andreeva, I.A., Ivanov, V.N., Petrova, V.I., 2004. The geotectonic nature of the Central Arctic morphostructures and geological implications of bottom sediments for its interpretation. Geotectonics 38, 430–442.
Karasik, A.M., Gurevich, N.I., Masolov, V.N., Schelovanov, V.G., 1971. Some features of a deep structure and an origin of Lomonosov Ridge on the aeromagnetic data, Geofiz. Metody Razvedki v Arktike 6, 9–19 (in Russian).
Korenaga, J., Holbrook, W.S., Kent, G.M., Kelemen, P.B., Detrick, R.S., Larsen, H.-C., Hoppes, J.R., Dahl-Jenssen, T., 2000. Crustal structure of the southeast Greenland margin from joint refraction and reflection seismic tomography. J. Geophys. Res. 105, 21,591–21,614.
Kovacs, L.C., Vogt, P.R., 1982. Depth-to-magnetic source analysis of the Arctic Ocean region. Tectonophysics 89, 255–294.
Lane, L.S., 1997. Canada Basin, Arctic Ocean: evidence against a rotational origin. Tectonics 16, 363–387.
Langinen, A.E., Gee, D.G., Lebedeva-Ivanova, N.N., Zamansky, Y.Y., 2006. Velocity structure and correlation of the sedimentary cover on the Lomonosov Ridge and in the Amerasian Basin, Arctic Ocean. In: Scott, R.A., Thurston, D.K. (Eds.), Proceedings of the Fourth International Conference on Arctic Margins, OCS Study MMS 2006-003. U.S. Department of the Interior, pp. 179–188.
Langinen, A.E., Lebedeva-Ivanova, N.N., Gee, D.G., Zamansky, Y.Y., 2009. Correlations between the Lomonosov Ridge, Marvin Spur and adjacent basins of the Arctic Ocean based on seismic data. Tectonophysics 472, 309–322.
Lawver, L.A., Scotese, C.R., 1990. A review of tectonic models for the evolution of Canada Basin. In: Grantz, A., Johnson, L., Sweeney, J.F. (Eds.), The Geology of North America, The Arctic Ocean Region, Vol. L. The Geological Society of America, pp. 593–618.
Lawver, L.A., Grantz, A., Gahagan, L.M., 2002. Plate kinematic evolution of the present Arctic region since the Ordovician. Spec. Pap. Geol. Soc. Am. 360, 333–358.
Laxon, S., McAdoo, D., 1994. Arctic Ocean gravity field derived from ERS-1 satellite altimetry. Science 265, 621–624.

Lebedeva-Ivanova, N., Lizarralde, D., 2011. An empirical direct-wave traveltime equation for Arctic sonobuoy data. Abstract. Sixth International Conference on Arctic Margins, ICAM VI. Geophysical Institute, University of Alaska Fairbanks, Fairbanks, AK, USA.
Lebedeva-Ivanova, N.N., Zamansky, Y., Langinen, A., Sorokin, M., 2006. Seismic profiling across the Mendeleev Ridge at 82°N: evidence of continental crust. Geophys. J. Int. 165, 527–544.
Lebedeva-Ivanova, N.N., Gee, D.G., Sergeyev, M.B., 2011. Crustal structure of the East Siberian continental margin, Podvodnikov and Makarov basins, based on refraction seismic data (TransArctic 1989–1991). Geol. Soc. Lond. Mem. 35, 395–411.
Ludwig, W.J., Nafe, J.E., Drake, C.L., 1970. Seismic refraction. In: Maxwell, A.E. (Ed.), The Sea, 4. Wiley-Interscience, New York, pp. 53–84.
Maher Jr., H.D., 2001. Manifestations of the Cretaceous High Arctic large igneous province in Svalbard. J. Geol. 109, 91–104.
Mayer, L.A., Armstrong, A.A., 2008. U.S. Law of the Sea cruise to map the foot of the slope and 2500-m isobath of the US Arctic Ocean margin report for 2008. Center for Coastal and Ocean Mapping. Paper 1258 (179 pp.).
Mayer, L.A., Armstrong, A.A., 2011. U.S. Law of the Sea cruise to map the foot of the slope and 2500-m isobath of the US Arctic Ocean margin. Center for Coastal and Ocean Mapping. Paper 1253 (235 pp.).
Mayer, L.A., Armstrong, A.A., 2012. U.S. Law of the Sea cruise to map the foot of the slope and 2500-m isobath of the US Arctic Ocean margin. Center for Coastal and Ocean Mapping. Paper 1282 (159 pp.).
Mayer, L.A., Calder, B., Mosher, D.C., 2016. U.S. Law of the Sea cruise to map and sample the U.S. Arctic Ocean margin, Healy 1603. Center for Coastal and Ocean Mapping (135 pp.).
Miller, E.L., Verzhbitsky, V., 2009. Structural studies in the Pevek region, Russia: implications for the evolution of the East Siberian Shelf and Makarov Basin of the Arctic Ocean. Stephan Mueller Publication Series 4, pp. 223–241.
Mjelde, R., Raum, T., Myhren, B., Shimamura, H., Murai, Y., Takanami, T., Karpuz, R., Næss, U., 2005. Continent ocean-transition on the Vøring Plateau, NE Atlantic, derived from densely sampled ocean bottom seismometer data. J. Geophys. Res. 110, 1–19.
Morozov, A.F., Petrov, O.V., Shokalsky, S.P., Kashubin, S.N., Kremenetsky, A.A., Shkatov, M.Y., Kaminsky, V.D., Gusev, E.A., Grikurov, G.E., Rekant, P.V., Shevchenko, S.S., Sergeev, S.A., Shatov, V.V., 2013. New geological data are confirming continental origin of the central Arctic rises. Reg. Geol. Metallog. 53 (in Russian).
Mosher, D.C. (Ed.), 2012. 2011 Canadian High Arctic seismic expedition: CCGS Louis S. St-Laurent expedition report. Geol. Surv. Can. 6343. Open File (266 pp.).
Mosher, D.C., Shimeld, J., Hutchinson, D., Chian, D., Lebedova-Ivanova, N., Jackson, R., 2012. Canada Basin Revealed. Proceedings of the 2012 Arctic Technology Conference. :pp. 1–11 http://dx.doi.org/10.4043/23797-ms.
Mosher, D.C., Chapman, C.B., Shimeld, J., Jackson, H.R., Chian, D., Verhoef, J., Pederson, R., 2013. High Arctic marine geophysical data acquisition. Lead. Edge 32, 524–536.
Mosher, D.C., Shimeld, J.W., Hutchinson, D.R., Jackson, H.R., 2016. Canadian UNCLOS Extended Continental Shelf Program seismic data holdings (2006–2011). Geological Survey of Canada, Open File 7938, 1. Zip File http://dx.doi.org/10.4095/297590.
Mudie, P.J., Blasco, S.M., 1985. Lithostratigraphy of the CESAR Cores. In: Jackson, H.R., Mudie, P.J., Blasco, S.M. (Eds.), Initial Geological Data Report on CESAR, The Canadian Expedition to Study the Alpha Ridge, Arctic Ocean. Geological Survey of Canada, Ottawa, Geological Survey of Canada Paper vols. 84–22, pp. 59–99.
Nafe, J.E., Drake, C.L., 1961. Physical properties of marine sediments. Tech. Rep. 2. Lamont-Doherty Geol. Observ., Palisades, N.Y. (29 pp.).
Oakey, G.N., Saltus, R.W., 2016. Geophysical analysis of the Alpha–Mendeleev ridge complex: characterization of the High Arctic Large Igneous Province. Tectonophysics 691, 65–84.
Operto, S., Charvis, P., 1995. Kerguelen Plateau: a volcanic passive margin fragment? Geology 23, 137–140.
Osler, J.C., 1993. Crustal Structure of the Extinct Spreading Center in the Labrador Sea: Implications for Dynamic Models of Flow Beneath Mid-ocean Ridges. (Ph.D. thesis). Dalhousie Univ., Halifax, Nova Scotia, Canada.
Passey, S.R., Bell, B.R., 2007. Morphologies and emplacement mechanisms of the lava flows of the Faroe Island Basalt Group, Faroe Islands, NE Atlantic Ocean. Bull. Volcanol. 70, 139–156.
Pease, V., Chev, S., Stephenson, R., Zhang, X., Pease, V., Zhang, X., 2014. Arctic lithosphere — a review. Tectonophysics 628, 1–25.
Petrov, O., Morozov, A., Shokalsky, S., Kashubin, S., Artemieva, I.M., Sobolev, N., Petrov, E., Richard, E.E., Sergeev, S., Smelror, M., 2016. Crustal structure and tectonic model of the Arctic region. Earth Sci. Rev. 154, 29–71.
Pietsch, R., Uenzelmann-Neben, G., 2015. The Manihiki Plateau—a multistage volcanic emplacement history. Geochem. Geophys. Geosyst. 16:2480–2498. http://dx.doi.org/10.1002/2015GC005852.
Pollack, H.N., Hurter, S.J., Johnson, J.R., 1993. Heat flow from the Earth's interior: analysis of the global data set. Rev. Geophys. 31, 267–280.
Poselov, V.A., Avetisov, G.P., Butsenko, V.V., Zholondz, S.M., Kaminsky, V.D., Pavlov, S.P., 2012. The Lomonosov Ridge as a natural extension of the Eurasian continental margin into the Arctic Basin. Russ. Geol. Geophys. 53, 1276–1290.
Salisbury, M.H., Christensen, N.I., 1978. The seismic velocity structure of a traverse through the Bay of Islands ophiolite complex, Newfoundland, an exposure of oceanic crust and upper mantle. J. Geophys. Res. 83, 805–817.
Saltus, R.W., Miller, E.L., Gaina, C., Brown, P.J., 2011. Regional magnetic domains of the Circum-Arctic: a framework for geodynamic interpretation. In: Spencer, A.M., Embry, A.F., Gautier, D.L., Stoupakova, A.V., Sørensen, K. (Eds.), Arctic Petroleum Geology: Geol. Soc. London, Memoirs 35, pp. 49–60.
Schlanger, S.O., Jackson, E.D., Boyce, R.E., Cook, H.E., Jenkyns, H.C., Johnson, D.A., et al., 1976. Site 317. Texas A & M University, Ocean Drilling Program, College Station, TX, United States http://dx.doi.org/10.2973/dsdp.proc.33.105.1976.
Sheriff, R.E., Geldart, L.P., 1995. Exploration Seismology. Cambridge University Press (592 pp.).
Shimeld, J., 2011. Chapter 2: acquisition and processing of the seismic reflection data. In: Mosher, D.C., Shimeld, J.W., Chapman, C.B. (Eds.), 2010 Canada Basin Seismic Reflection and Refraction Survey, Western Arctic Ocean: CCGS Louis S. St-Laurent Expedition Report, Geological Survey of Canada, Open File vol. 6720, pp. 49–68.
Shimeld, J., Li, Q., Chian, D., Lebedeva-Ivanova, N.N., Jackson, H.R., Mosher, D.C., Hutchinson, D.R., 2016. Seismic velocities within the sedimentary succession of the Canada Basin and southern Alpha-Mendeleev Ridge, Arctic Ocean: evidence for accelerated porosity reduction? Geophys. J. Int. 204, 1–20.
Stanghellini, G., Bonazzi, C., 2002. Local-trace zeroing and spike zeroing: two short automated noise-rejection routines to remove noise and spikes on seismic traces. Geophysics 67, 188–196.
Sweeney, J.F., Weber, J.R., Blasco, S.M., 1982. Continental ridges in the Arctic Ocean: LOREX constraints. Tectonophysics 89, 217–237.
Talwani, M., Worzel, J.L., Landisman, M., 1959. Rapid gravity computations for two-dimensional bodies with application to the Mendocino submarine fracture zone. J. Geophys. Res. 64, 49–59.
Tegner, C., Storey, M., Holm, P.M., Thorarinsson, S.B., Zhao, X., Lo, C.H., Knudsen, M.F., 2011. Magmatism and Eurekan deformation in the High Arctic Large Igneous Province: ^{40}Ar–^{39}Ar age of Kap Washington Group volcanics, North Greenland. Earth Planet. Sci. Lett. 303, 203–214.
Todd, B.J., Reid, I., Keen, C.E., 1988. Crustal structure across the Southwest Newfoundland Margin. Can. J. Earth Sci. 25, 744–759.
Van Wagoner, N.A., Williamson, M.-C., Robinson, P.T., Gibson, I.L., 1986. First samples of acoustic basement recovered from the Alpha Ridge, Arctic Ocean: new constraints for the origin of the ridge. J. Geodyn. 6, 177–196.
Vogt, P.R., Taylor, P.T., Kovacs, L.C., Johnson, G.L., 1979. Detailed aeromagnetic investigations of the Arctic Basin. J. Geophys. Res. 84, 1071–1089.
Vogt, P.R., Taylor, P.T., Kovacs, L.C., Johnson, G.L., 1982. The Canada Basin: aeromagnetic constraints on structure and evolution. Tectonophysics 89, 295–336.
Vogt, P.R., Jung, W.-Y., Jakobsson, M., Mayer, L., Williamson, M., 2006. The Alpha-Mandeleev magmatic province, Arctic Ocean– a new synthesis. EOS 87, 36 (Abs.).
Weber, J.R., 1990. The structures of the Alpha Ridge, Arctic Ocean and Iceland-Faeroe Ridge, North Atlantic; comparisons and implications for the evolution of the Canada Basin. Mar. Geol. 93, 43–68.
Weigelt, E., Jokat, W., 2001. Peculiarities of roughness and crustal thickness of oceanic crust in the Eurasian Basin, Arctic Ocean. Geophys. J. Int. 145, 505–516.
Weigelt, E., Franke, D., Jokat, W., 2014. Seismostratigraphy of the Siberian Arctic Ocean and adjacent Laptev Sea Shelf. J. Geophys. Res. 119:5275–5289. http://dx.doi.org/10.1002/2013JB010727.
White, R.S., Mackenzie, D., O'Nions, R.K., 1992. Oceanic crustal thickness from seismic measurements and rare earth element inversions. J. Geophys. Res. 9 (B13), 19,683–19,715.
Wilkens, R.H., Fryer, G.J., Karsten, J., 1991. Evolution of porosity and seismic structure of upper oceanic crust: importance of aspect ratios. J. Geophys. Res. 96, 17,981–17,995.
Zelt, C.A., 1994. Software Package ZPLOT. Bullard Laboratories, University of Cambridge.
Zelt, C.A., Smith, R.B., 1992. Seismic traveltime inversion for 2-D crustal velocity structure. Geophys. J. Int. 108, 16–34.